THE JOURNAL OF BIOLOGICAL CHEMISTRY VOL. 284, NO. 43, pp. 29757–29772, October 23, 2009

Cyanochromes Are Blue/Green Light Photoreversible Photoreceptors Defined by a Stable Double Cysteine Linkage to a Phycoviolobilin-type Chromophore*[S]◆

Received for publication, June 29, 2009, and in revised form, August 3, 2009 Published, JBC Papers in Press, August 11, 2009, DOI 10.1074/jbc.M109.038513

Andrew T. Ulijasz[‡1], Gabriel Cornilescu[§], David von Stetten[¶], Claudia Cornilescu[§], Francisco Velazquez Escobar[¶], Junrui Zhang[‡], Robert J. Stankey[‡], Mario Rivera[‖], Peter Hildebrandt[¶], and Richard D. Vierstra[‡2]

From the [‡]Department of Genetics, University of Wisconsin, and the [§]National Magnetic Resonance Facility at Madison, Madison, Wisconsin 53706, the [¶]Technische Universität Berlin, D-10623 Berlin, Germany, and the [‖]Department of Chemistry, University of Kansas, Lawrence, Kansas 66045

Phytochromes are a collection of bilin-containing photoreceptors that regulate a diverse array of processes in microorganisms and plants through photoconversion between two stable states, a red light-absorbing Pr form, and a far red light-absorbing Pfr form. Recently, a novel set of phytochrome-like chromoproteins was discovered in cyanobacteria, designated here as cyanochromes, that instead photoconvert between stable blue and green light-absorbing forms Pb and Pg, respectively. Here, we show that the distinctive absorption properties of cyanochromes are facilitated through the binding of phycocyanobilin via two stable cysteine-based thioether linkages within the cGMP phosphodiesterase/adenyl cyclase/FhlA domain. Absorption, resonance Raman and infrared spectroscopy, and molecular modeling of the *Te*-PixJ GAF (cGMP phosphodiesterase/adenyl cyclase/FhlA) domain assembled with phycocyanobilin are consistent with attachments to the C3[1] carbon of the ethylidene side chain and the C4 or C5 carbons in the A–B methine bridge to generate a double thioether-linked phycoviolobilin-type chromophore. These spectroscopic methods combined with NMR data show that the bilin is fully protonated in the Pb and Pg states and that numerous conformation changes occur during Pb → Pg photoconversion. Also identified were a number of photochromically inactive mutants with strong yellow or red fluorescence that may be useful for fluorescence-based cell biological assays. Phylogenetic analyses detected cyanochromes capable of different signaling outputs in a wide range of cyanobacterial species. One unusual case is the *Synechocystis* cyanochrome Etr1 that also binds ethylene, suggesting that it works as a hybrid receptor to simultaneously integrate light and hormone signals.

Phytochromes (Phys)[3] comprise a large and diverse superfamily of photoreceptors that regulate a wide range of physiological responses in plants, fungi, bacteria, and cyanobacteria (1–3). They are unique among photoreceptors by being able to photoconvert between two stable states, a red light-absorbing Pr form that is typically the dark-adapted and biologically inactive conformer and a far-red light-absorbing Pfr form that requires light for its production and is typically the biologically active conformer. By interconverting between Pr and Pfr, Phys act as light-regulated switches in controlling processes ranging from phototaxis and pigmentation in bacteria to seed germination, photomorphogenesis, and flowering time in higher plants.

Light absorption by Phys is directed by a bilin (or linear tetrapyrrole) chromophore produced by the oxidative cleavage of heme. Although bacterial and fungal Phys use the immediate cleavage product biliverdin (BV), cyanobacterial and higher plant Phys use phycocyanobilin (PCB) and phytochromobilin, respectively, produced by enzymatic reduction of BV (1, 2). The bilin is then covalently bound autocatalytically to the photosensory unit of the apoprotein, which typically contains a sequence of Per/Arndt/Sim (PAS), cGMP phosphodiesterase/adenyl cyclase/FhlA (GAF), and Phy-associated (PHY) domains. Intimate contact between the bilin and surrounding protein residues then generates the unique photochromic properties of Phys. Recent three-dimensional structures of the Pr form of several bacterial Phys (BphPs) and two cyanobacterial Phys (Cphs) have shown that the bilin is deeply buried within the GAF domain in a *ZZZssa* configuration and that the connection between the GAF and PAS domains is stabilized by a rare figure-of-eight knot involving the region upstream of the PAS domain being lassoed by a conserved loop within the GAF domain (4–9). Although the structure of Pfr remains unsolved, various physicochemical studies have proposed that photoconversion involves a rotation of one of the three methine bridges between the pyrrole rings (1, 10–14). This rotation then

* This work was supported by National Science Foundation Grant MCB 07191530 (to R. D. V.) and Deutsche Forschungsgemeinschaft Grant SFB498 (to P. H.).

◆ This article was selected as a Paper of the Week.

[S] The on-line version of this article (available at http://www.jbc.org) contains supplemental Tables 1–3 and Figs. 1–6.

[1] Recipient of an American Heart Association postdoctoral fellowship.

[2] To whom correspondence should be addressed: Dept. of Genetics, 425-G Henry Mall, University of Wisconsin-Madison, Madison, WI 53706. Tel.: 608-262-8215; Fax: 608-262-2976; E-mail: vierstra@wisc.edu.

[3] The abbreviations used are: Phy, phytochrome; PHY, Phy-associated domain; BphP, bacteriophytochrome; Cph, cyanobacterial phytochrome; Pb, blue light-absorbing form of cyanochrome; Pg, green light-absorbing form of cyanochrome; Pfr, far-red light-absorbing form of Phy; Pr, red light-absorbing form of Phy; BV, biliverdin IXα; Cyc, cyanochrome; GAF, cGMP phosphodiesterase/adenyl cyclase/FhlA; HK, histidine kinase; HSQC, heteronuclear single quantum coherence; IR, infrared; PAS, Per/Arndt/Sim; PCB, phycocyanobilin; PVB, phycoviolobilin; PEB, phycoerythrobilin; PUB, phycourobilin; ALA, α-aminolevulinic acid; RR, resonance Raman; Ni-NTA, nickel-nitrilotriacetic acid; *SyB*, *Synechococcus* sp. OS-B′; *Syn*, *Synechocystis* sp. PCC6803; *Te*, *Thermosynechococcus elongatus* BP-1; *Dr*, *Deinococcus radiodurans*.

induces much slower thermally driven movements of the protein to initiate signal transduction.

In microorganisms, Pfr can activate a variety of signaling systems using output motifs directly appended to the C-terminal end of the photosensory region. The most prevalent are histidine kinase domains that then begin specific two-component phosphorelays (3, 15, 16). Although the output of plant Phys remains unclear, the presence of a C-terminal HK-related domain suggests that they also work as light-regulated protein kinases (17).

In addition to the canonical Phys, it has become apparent through phylogenetic and biochemical studies that a heterogeneous collection of Phy-like photoreceptors exists (*e.g.* Refs. 3 and 18). These include Phys that prefer Pfr as the dark-adapted state (7, 19, 20), Phys that photoconvert from Pr to shorter wavelength-absorbing "near red" or Pnr forms (6, 21), and Phy-like photoreceptors that bind bilins but instead photoconvert between forms with maximal absorption other than red and far-red light (22–25). Often these Phy-like sequences are missing key residues or domains common among canonical Phys, suggesting that they employ novel bilins as chromophores, bind the bilin in different architectures, and/or use distinct photochemistries.

One subclass of novel Phy-like photoreceptors present in a number of cyanobacteria, which we have designated cyanochromes (or Cycs) to better distinguish them from Cphs, is exemplified by *Synechocystis* sp. PCC6803 (*Syn*) PixJ (or TaxD1, locus *sll0041*) and its relatives. *Syn*-PixJ was discovered based on its involvement in blue light-mediated phototaxis in this mesophilic cyanobacterium (26, 27) with its close homolog *Te*-PixJ (locus *tll0569*) then found in the thermophilic cyanobacterium *Thermosynechococcus elongatus* BP-1 by sequence similarity (28). Like Cphs, the cyanochromes tested thus far covalently bind PCB but then generate photoreceptors that convert between blue and green light-absorbing forms designated Pb and Pg, respectively (22, 24, 29). Subsequent studies proposed that PCB is converted to phycoviolobilin (PVB) upon attachment to the apoprotein (30). PVB differs from PCB by having a methylene instead of a methine bridge between the A and B pyrrole rings, which blue-shifts the absorption of the chromophore by shortening the π-conjugation system. Phototransformation of Pb to Pg could then occur by a mechanism similar to Phys.

How *Te*-PixJ and related cyanochromes bind PCB to generate more blue-shifted PVB-type chromophores remains unclear. Like Cphs, two cyanochromes examples link PCB via a thioether linkage between a cysteine in the Cyc-GAF domain and the $C3^1$ carbon of the ethylidene side chain of ring A (24, 28). Additionally, loss of the C4=C5 double bond is necessary to generate PVB. One model by Ishizuka *et al.* (30) from studies with *Te*-PixJ proposed that the double bond moves from the C4-C5 position to the C2-C3 position by an autoisomerase activity intrinsic to the GAF domain. A more recent model by Rockwell *et al.* (24) using another *Syn*-PixJ relative in *T. elongatus*, Tlr0924, invoked the possibility of a second cysteine that also participates in PCB ligation. This cysteine was proposed to bind the bilin at the C10 position via a reversible thioether linkage. In the dark-adapted Pb state, the second linkage would then be formed to generate a rubin-like chromophore attached to the bridge between the B and C pyrrole rings. This bond would then break upon photoconversion to generate the more π-conjugated green light-absorbing photoproduct Pg.

In this report, we employed a number of physicochemical approaches to help resolve the unique chromophore architecture and photochemical properties of cyanochromes, using *Te*-PixJ as the example. By independently mutagenizing the cysteine that binds the A ring ethylidene (Cys-522 (22)) and that proposed by Rockwell *et al.* (24) to reversibly bind the bilin at a second site (Cys-494), we demonstrate that both residues form light-stable covalent adducts with a PVB-type chromophore. In addition, we employed various spectroscopic methods to show that the bound PVB is fully protonated as both Pb and Pg, that only one pyrrole ring is active during photoconversion, and that the polypeptide may undergo extensive remodeling as Pb converts to Pg. We identified a set of conserved amino acids in *Te*-PixJ important for cyanochrome photochemistry, including several that when substituted generate yellow or red fluorescent chromoproteins potentially useful for cell biological applications. Phylogenetic analyses show that cyanochromes are widespread among cyanobacteria with their closest relatives being members of the red/far-red light-absorbing Phy subfamily defined by the absence of the N-terminal PAS domain (31).

EXPERIMENTAL PROCEDURES

Te-PixJ Cyc-GAF Domain Alignment and Secondary and Tertiary Structure Predictions—Phy/Cyc sequences were identified by performing BLAST searches of the GenBank™ data base (www.ncbi.nlm.nih.gov) using the *Te*-PixJ Cyc-GAF domain sequence as the query. Amino acid sequence alignments were generated with ClustalW (32) and displayed using MacBoxShade version 2.15 (Institute of Animal Health, Pirbright, UK). Secondary structure was predicted using the Scratch Protein Predictor (SSpro) (33, 34). The tertiary structure of *Te*-PixJ(Cyc-GAF) was predicted using the SWISS-MODEL online resource (35) by inputting an alignment of the *SyB*-Cph1 GAF domain (Leu-31 to Gln-200) and *Te*-PixJ Cyc-GAF domain (Arg-440 to Phe-585) sequences along with the three-dimensional structure of *SyB*-Cph1(GAF) as the molecular template (Protein Data Bank (PDB) ID code 2K2N (8)). Representations of the predicted *Te*-PixJ(Cyc-GAF) structure were generated by PyMOL (DeLano Scientific LLC, San Carlos, CA).

Phylogenetic Analysis—Phy, Cyc and related sequences were obtained from the National Center for Biotechnology Information (NCBI) and the Joint Genomes Institute (JGI) data bases and are listed with their accession numbers in supplemental Table 1. Sequences were aligned using CLUSTALX (36) under default settings and trimmed to include only the GAF domain (supplemental Table 2). Phylogenetic analysis was performed with MrBayes version 3.1.2 (37) using the proportion of invariable sites γ rate model and the mixed amino acid model. The software was run for 1,350,000 generations, discarding the first 25% (337,500 generations) as "burn-in" after checking that the log likelihood values had plateaued. The strict consensus tree was displayed with TreeView (38). A similar tree architecture

was produced using the PROTML application in the PHYLIP package (39).

Expression of Recombinant Cyc-GAF Domains—The coding regions for the Cyc-GAF domain from *Te*-PixJ (residues 430–591 from locus *tll0569*) and *Syn*-Etr1 (residues 466–624 from locus *slr1212*) were PCR-amplified from *T. elongatus* BP-1 genomic DNA and the *Synechocystis* plasmid pYCDE (40), respectively, and cloned into NcoI/HindIII-digested pBAD-6H expression plasmid using the melt and reanneal method as described (31). *Te*-PixJ(Cyc-GAF) mutants were generated by PCR as described (31), using two complementary primers containing the desired nucleotide change. Primers used in this study are shown in supplemental Table 3.

Recombinant GAF domain expression and purification were performed as described previously (31) using a modification of the dual plasmid expression system devised by Gambetta and Lagarias (41). For *in vitro* assembly, *Escherichia coli* crude extracts containing the apoprotein were incubated with 200 μM protoporphyrin IXα, BV, or PCB at 4 °C for 4 h prior to purification. Bilin incorporation was assayed by zinc-induced fluorescence of the chromoproteins following SDS-PAGE (15, 29). The zinc-impregnated gels were irradiated with UV light with the fluorescence emission detected in the visible region of the light spectrum.

To isotopically label PCB with ^{13}C at carbons 4, 5, 9, 10, 11, 15, and 19 prior to assembly with the *Te*-PixJ(Cyc-GAF) apoprotein, 100 μM 5-[^{13}C]α-aminolevulinic acid (ALA) was added to the minimal expression medium as described (31). Incorporation of ^{15}N into PCB was similarly accomplished by adding a final concentration of 100 μM [^{15}N]ALA (Medical Isotopes Inc., Pelham, NH). Following a 2-h induction of the *E. coli* BL21-AI cultures with 1 mM isopropyl 1-thio-β-D-galactopyranoside and an overnight induction at 18 °C with 0.2% arabinose, the expressed proteins were purified by nickel nitrilotriacetic acid agarose (Ni-NTA) chromatography (Qiagen, Valencia CA), using 300 mM imidazole for elution. Most eluates were then dialyzed into 25 mM Tris-HCl (pH 8.0) using Amicon Ultra-15 centrifugal filters (10 kDa cutoff, Millipore, Billerica, MA), with the exception of samples used for resonance Raman (RR) or IR spectroscopy, which were dialyzed into 25 mM Tris-HCl (pH 8.0) and 1 mM EDTA. Samples for NMR analysis were further purified by fast protein liquid chromatography with a phenyl-HP column (GE Healthcare) (31), pooled, and then dialyzed into 10 mM Tris-DCl (pH 8.0). 5-[^{13}C]ALA-labeled *Te*-PixJ(GAF) was adjusted to a final concentration of 1.3 mM for IR and RR spectroscopy and a final concentration of 1.75 mM for NMR spectroscopy. The [^{15}N]ALA-labeled *Te*-PixJ(GAF) samples were brought to a concentration of 1.5 mM before NMR analysis.

Absorption and Fluorescence Spectroscopy—Absorption spectra were measured with a PerkinElmer Lambda 650 UV-visible spectrometer (PerkinElmer Life Sciences) with the samples dissolved in 25 mM Tris-HCl (pH 8.0). Pb → Pg and Pg → Pb photoconversions were achieved with white light filtered through appropriate 430- and 530-nm interference filters, respectively. Pr → Pfr and Pfr → Pr photoconversions were achieved with white light filtered through 630- and 690-nm interference filters, respectively. For denaturation experiments, the chromoproteins were either photoconverted with white light and the appropriate interference filter (430 nm for Pb and 630 nm for Pr) or kept in darkness followed by denaturation in 8 M urea (pH 2.0). Soluble and bound chromophores were separated following 10% trichloroacetic acid precipitation. The precipitated fraction was redissolved in acidic urea. Following UV-visible absorption measurements, denatured samples were then irradiated with the appropriate wavelength of light corresponding to their Pb/Pr and Pg/Pfr peak absorbance as follows: wild-type *Te*-PixJ(Cyc-GAF) (590 and 530 nm), *Te*-PixJ(Cyc-GAF) D494H (590 and 660 nm), *Te*-PixJ(Cyc-GAF) C522A (590 or 690 nm), *Te*-PixJ(Cyc-GAF) C494A, and *SyB*-Cph1(GAF) (590 and 660 nm).

Fluorescence excitation and emission spectra were recorded with a QuantaMaster model C-60/2000 spectrofluorometer (Photon Technologies International, Birmingham, NJ). Emission spectra were recorded with an excitation of 523–555 nm, depending on the sample. Wild-type *Te*-PixJ(Cyc-GAF) and the Y463H, D492H, and C522A mutants were excited with 360 nm light, and the C494H and C494A mutants were excited with 590 nm light. Excitation spectra were recorded with 551–651-nm emission wavelengths, depending on the sample.

RR Spectroscopy—RR spectra were recorded with 1064 nm excitation (Nd-YAG continuous wave laser, line width <1 cm^{-1}) using a RFS 100/S (Bruker Optics, Ettlingen, Germany) Fourier transform Raman spectrometer (4 cm^{-1} spectral resolution). The near IR excitation line was sufficiently close to the first electronic transition to generate a strong preresonance enhancement of the chromophoric vibrational bands such that Raman bands of the protein matrix remained very weak in the spectra of the parent states (42–44). Typical sample volumes were 5 μl of a 1–2 mM protein solution in 25 mM Tris-HCl (pH 8.0) and 1 mM EDTA. All spectra were measured at −140 °C using a liquid-nitrogen cooled cryostat (Linkam, Waterfield, Surrey, UK). The laser power at the sample was set at ~700 milliwatts, which did not damage the chromoproteins as checked by comparing spectra of the samples obtained before and after RR data acquisition. The total accumulation time was less than 2 h for each spectrum. For all RR spectra, the background was subtracted manually. Calculated RR and IR spectra were obtained by density functional theory using the B3LYP functional and the 6–31G* basis set. The force field was scaled by a set of global scaling factors as described elsewhere (13, 45). To detect photoproducts that accumulate in blue light, the samples were irradiated at room temperature and then rapidly frozen to −140 °C. Green light-emitting diodes combined with a blue interference filter were used for photoconversion in the RR and IR experiments.

IR Spectroscopy—IR difference spectra were recorded at 20 °C in a Bruker Tensor IR interferometer equipped with an attenuated total reflection device. Typical sample volumes were 20 μl of a 1–2 mM protein solution in 25 mM Tris-HCl (pH 8.0) and 1 mM EDTA. Composite spectra were assembled from 200 scans (~90 s each); these spectra were recorded in batches of five separated alternately by saturating green and blue light irradiations. Difference spectra from 10–15 blue/green irradiation cycles were generated and added together without background correction.

NMR Spectroscopy—Isotopically labeled forms of *Te*-PixJ-(Cyc-GAF) assembled with PCB (~2 mM) were dissolved in 93% H_2O, 7% D_2O, 10 mM deuterated Tris-DCl (pH 8.0), and 0.15 mM NaN_3 and placed in a 280-μl Shigemi microcell. NMR spectra were collected at 25 °C using an 800-mHz ^1H frequency Varian INOVA spectrometer (Varian Inc., Palo Alto, CA)

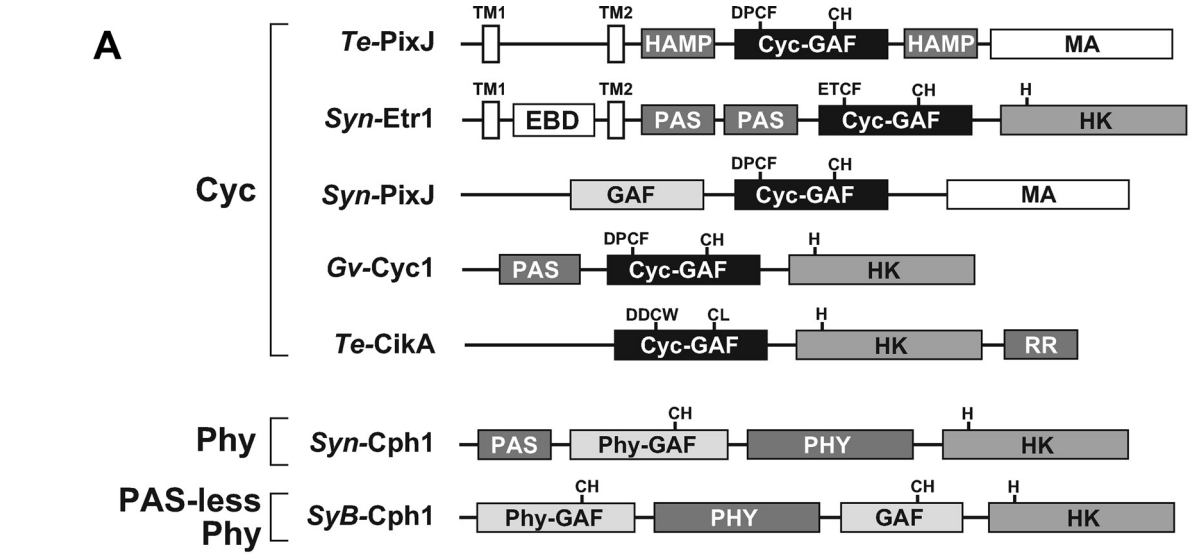

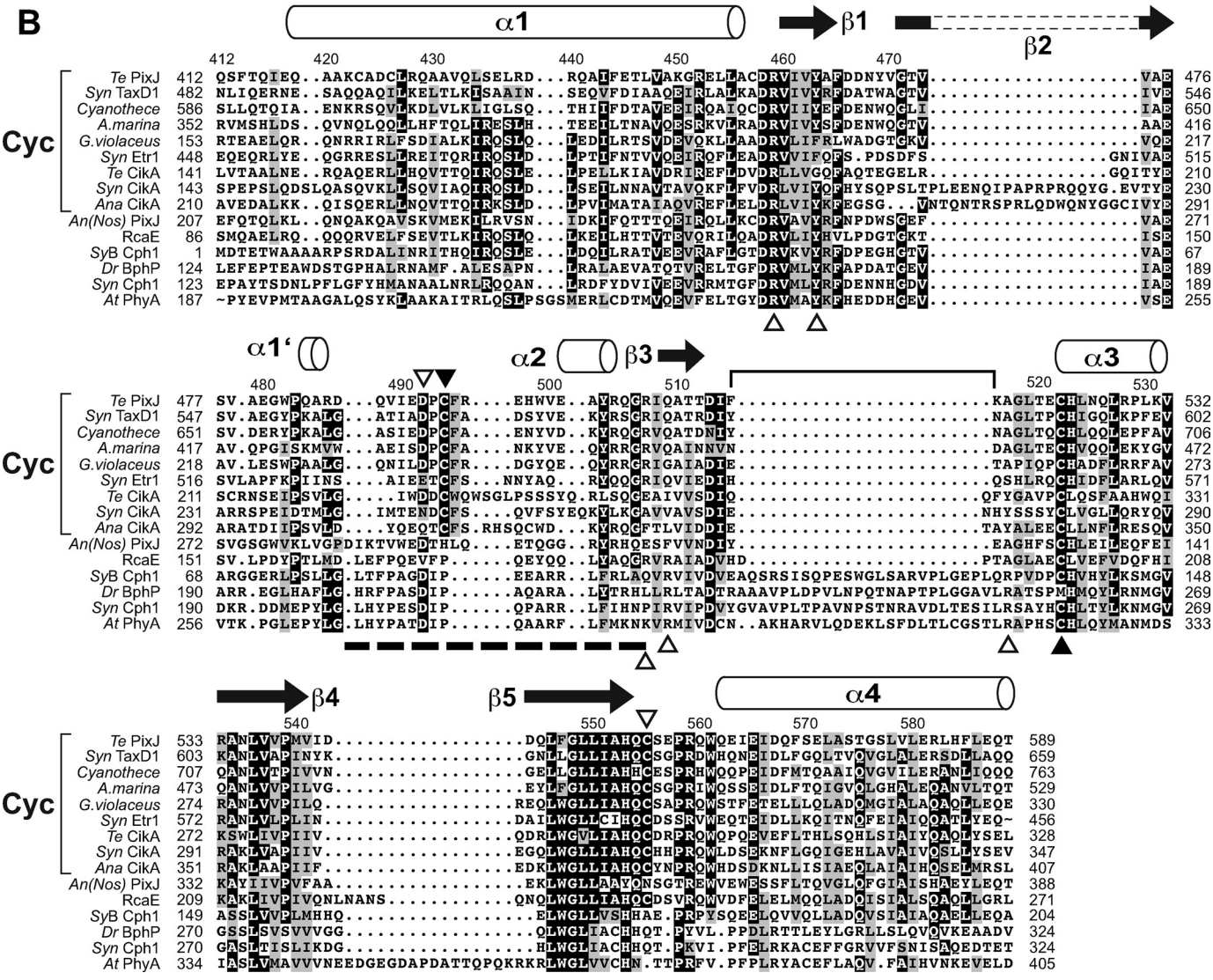

equipped with a cryogenic probe. Pg samples were obtained by irradiating the microcell solution with saturating blue light (430 nm). Photoconversion of Pg → Pb was accomplished by irradiating the microcell with saturating green light (530 nm).

^{1}H-^{15}N heteronuclear single quantum coherence (HSQC) spectra with ^{15}N-^{13}C-labeled *Te*-PixJ(Cyc-GAF) chromoprotein or unlabeled *Te*-PixJ(Cyc-GAF) protein assembled with [^{15}N]PCB were collected as 128*(t_1, ^{15}N) × 1022* (t_2, ^{1}H) data matrices. Acquisition times were 48 and 85 ms in the t_1 and t_2 dimensions, respectively. ^{1}H-^{13}C HSQC spectra, which centered on the methine region of unlabeled *Te*-PixJ(Cyc-GAF) protein assembled with [^{13}C]PCB, were collected as 32*(t_1, ^{13}C) × 769* (t_2, ^{1}H) data matrices. Acquisition times were 10 and 80 ms in the t_1 and t_2 dimensions, respectively. ^{13}C direct detected spectra were acquired with 51,200 scans and a total experimental time of 23 h each. Data were processed and plotted using the NMRPipe software package (46). All NMR data were collected at the National Institutes of Health-sponsored National Magnetic Resonance Facility at Madison (NMRFAM) at the University of Wisconsin.

RESULTS

Architecture and Phylogeny of Cyanochromes—PixJ-type biliproteins represent a novel class of Phy-type photoreceptors that photoconvert between blue (Pb) and green light-absorbing (Pg) forms (22, 28). To better define their distribution, we used the Cyc-GAF domain sequences of *Syn*-PixJ (TaxD1) and *Te*-PixJ to search the various genome data bases for potential homologs. This search retrieved numerous relatives in a variety of cyanobacteria, including *T. elongatus*, *Synechocystis*, *Cyanothece*, *Acaryochloris marina*, *Gloeobacter violaceus*, *Anabaena variabilis*, and *Anabaena* (*Nostoc*) species, (Fig. 1*B* and supplemental Table 1). Previously known Phy-type proteins that also clustered in this group included: *Synechococcus elongatus* CikA (involved in circadian entrainment (47)) and *Synechocystis* Etr1 (implicated in ethylene perception (40)), suggesting that these proteins are photochemically related to PixJ. No PixJ-type sequences were found in any species outside of cyanobacteria, in agreement with the prediction that this photoreceptor type is restricted to the cyanobacterial kingdom (24, 29). Consequently, we have used the term cyanochromes (or Cycs) to name this unique group to better distinguish them from the more typical Cphs that are present together with Cycs in many cyanobacterial species.

When the obtained GAF domain sequences were analyzed using a Bayesian phylogenetic comparison, the resultant cyanochrome clade was clearly separate from others in the Phy superfamily, including BphPs, Cphs, diatom Phys (Dphs), fungal Phys (Fphs), and plant Phys (supplemental Fig. 1). Maximum likelihood-generated trees produced a similar result (data not shown). Their closest relatives appear to be the PAS-less Phys, the founding member of which is *Synechococcus OS* Type B′ (*SyB*)-Cph1 (8, 31). Members of this clade are missing the PAS domain that is upstream of the chromophore-binding GAF domain in other canonical Phys.

Alignment of the GAF sequence from various Phy types revealed a distinct organization for the cyanochrome family (Fig. 1*B* and supplemental Table 2). Most notable in cyanochromes is the absence of the ~23-amino acid region between the predicted β3 strand and the α3 helix in the Cyc-GAF sequences, which forms the lasso loop in the knot of canonical BphPs, Cphs, Fphs, and plant Phys (4). The DIP motif that participates in the hydrogen-bond network involving the pyrrole water in canonical Phys is also absent. Instead, we (like Rockwell *et al.* (24)) often found a DPCF or related ETCF motif at this position. Despite this divergence, several residues known to make important contacts with the bilin in canonical Phys are conserved in cyanochromes. These include the cysteine (Cys-522 in *Te*-PixJ) that likely binds PCB through the C3^{1} carbon on the A ring ethylidene side chain, two histidine residues (His-523 and His-553) that bind the pyrrole water and the D ring, respectively, a tyrosine (Tyr-463) that is in close proximity to D ring and important for photoconversion, and an arginine (Arg-507) that forms a double salt bridge with the B-ring propionic acid side chain of PCB (Fig. 1*B*) (4, 5, 24, 28), suggesting that cyanochromes interact non-covalently with the bilin in a manner similar to other Phys.

Like other Phy types (2, 3, 20, 31, 48), the cyanochromes have widely varied domain architectures N- and C-terminal to their signature Cyc-GAF domains (Fig. 1*A*) (29). Examples include *Te*-PixJ, which has two predicted transmembrane domains at the N-terminal end, two HK/adenyl cyclase/methyl-binding protein-phosphatase (HAMP) domains bracketing the Cyc-GAF domain, and a methyl-accepting (*MA*) domain at the C-terminal end, and *Syn*-Etr1, which has a predicted ethylene-binding domain between two transmembrane domains followed by two PAS domains and a typical HK domain at the C-terminal end. Cyanochromes are notable among the Phy superfamily for not having an obvious PHY domain following the Cyc-GAF domain. In agreement with their predicted phylogenetic relationship to PAS-less Phys based on the GAF

FIGURE 1. **Protein organization and GAF domain amino acid sequence alignment of representative Cycs.** *A*, domain architectures of representative Cycs as compared with the Cph *Syn*-Cph1 and the PAS-less Phy *SyB*-Cph1. *EBD*, ethylene-binding; *HAMP*, histidine kinase/adenyl cyclase/methyl-binding protein/phosphatase; *MA*, methyl-accepting; *TM*, predicted transmembrane. The motifs containing the cysteine(s) that bind(s) the bilin and the histidine in the HK domain that participates in phosphotransfer are indicated. *B*, alignment of the GAF domain from representative Cycs (*brackets*) with members of the BphP (*Dr*-BphP), Cph (*Syn*-Cph1), PAS-less Phy (*SyB*-Cph1), and plant Phy (*At*-PhyA) clades. The predicted α-helical and β strand secondary structures based on the *Dr*-BphP and *SyB*-Cph1 three-dimensional structures (5, 8) are shown above the alignment. The *bracket* locates the conserved knot lasso loop present in canonical Phys. The *dashed line* locates the Cyc-specific motif bearing the second bilin attachment site. The two cysteines (Cys-494 and Cys-522) that bind the bilin are indicated by the *closed arrowheads*. Other key residues, some of which impact the spectral properties of *Te*-PixJ, are indicated by the *open arrowheads*. The amino acid numbering refers to the *Te*-PixJ sequence. Sequences in the alignment include: *Te*-PixJ from *T. elongatus* BP-1 (Tll0569), *Syn*-PixJ(TaxD1) from *Synechocystis* sp. PCC6803 (Sll0041), ZP_01728273 from *Cyanothece* sp. CCY0110, AM1_0048 from *A. marina* (MBIC11017), Glr3432 from *G. violaceus* PCC7421, *Syn*-Etr1 from *Synechocystis* sp. PCC6803 (Slr1212), *Te*-CikA from *T. elongatus* BP-1 (Tll0899), *Syn*-CikA from *S. elongatus* (slr1969), *Ana*-CikA from *A. variabilis* ATCC 29413 (Ava_1168), *An(Nos)*-PixJ from *Anabena* (*Nostoc*) sp. PCC7120 (All1069), RcaE from *F. diplosiphon* (AAB08575), *SyB*-Cph1 from *Synechococcus* sp. JA-2-3B′a(2-13) (CYB_2465), *Dr*-BphP from *D. radiodurans* R1 (DR0050), *Syn*-Cph1 from *Synechocystis* sp. PCC6803 (Slr0473), and *At*-PhyA from *A. thaliana* Columbia-0 ecotype (At1g09570). The accession numbers or locus tags are in *parentheses*.

domain sequence, some members of the cyanochrome family also do not have an obvious PAS domain N-terminal to the Cyc-GAF domain. Consequently, the photosensory domain of some cyanochrome members may be the smallest known within the Phy superfamily, with only their Cyc-GAF domain potentially required for full blue/green light-driven photochromicity.

Te-PixJ Binds PCB via a Stable Double Cysteine Linkage—To examine the photochemistry of cyanochromes, we used a recombinant assembly protocol in which the Cyc-GAF domain from *Te*-PixJ was expressed in *E. coli* with a C-terminal His_6 tag and either assembled *in vitro* with purified bilins or assembled *in vivo* by co-expression with bilin synthetic enzymes (16, 31, 41). Bilin attachment was then assessed by zinc-induced fluorescence of the purified chromoproteins following SDS-PAGE. As shown in Fig. 2*A*, purified *Te*-PixJ(Cyc-GAF) showed a strong preference for PCB and failed to bind BV or the bilin precursor protoporphyrin IXα *in vitro*. However, PCB binding was poor, suggesting that its incorporation is inefficient post-translationally. In contrast, robust PCB incorporation was evident upon *in vivo* co-synthesis of *Te*-PixJ(Cyc-GAF) with the heme oxygenase and PCB synthase activities that sequentially convert heme into PCB (Fig. 2*B*). Like previous studies (22, 24, 28), we found that the recombinant wild-type Cyc-GAF domain assembled with PCB displayed a blue absorption maximum at 430 nm for the dark-adapted Pb state, which could then be photoconverted by blue light to the Pg state with an absorption maximum at 534 nm (Fig. 2*C*).

In agreement with Ishizuka *et al.* (28), we found that Cys-522 is important for bilin attachment as its replacement with alanine substantially diminished PCB incorporation. However, PCB still bound (albeit poorly) with the assembled chromoprotein acquiring a new absorption maximum at ~600 nm in addition to the blue light maximum at 430 nm (Fig. 2, *B* and *C*). It also remained photochromic with blue light increasing its absorbance at 600 nm and shifting the blue light maximum to 370 nm. Taken together, the data implied that a second PCB-ligation site exists.

To locate other residues that could generate a second thioether linkage, we scanned our sequence alignment of the Cyc-GAF domains for additional conserved cysteines. One obvious candidate was Cys-494, which is present within the DPCF or related sequence in the cyanochrome clade (Fig. 1*B*). Importantly, we (like Rockwell *et al.* (24)) found that this sequence aligned with the DIP motif in canonical Phys, thus placing Cys-494 close to the chromophore based on the three-dimensional structures of the PAS-less Phy *SyB*-Cph1 (8). When tested recombinantly, we found that Cys-494 also contributes to bilin attachment; its replacement with alanine compromised chromoprotein assembly and prevented the residual chromoprotein from photoconversion (Fig. 2, *B* and *C*). Strikingly, the absorption maximum of the C494A mutant was remarkably similar to the PAS-less Phy *SyB*-Cph1(GAF) assembled with PCB (Fig. 2*C* and supplemental Fig. 2), suggesting that the chromophore was no longer PVB but PCB as predicted if a second binding site was eliminated. Analysis of a double cysteine mutant (C494A/C522A) then confirmed that both residues together are essential for proper PCB attachment. The

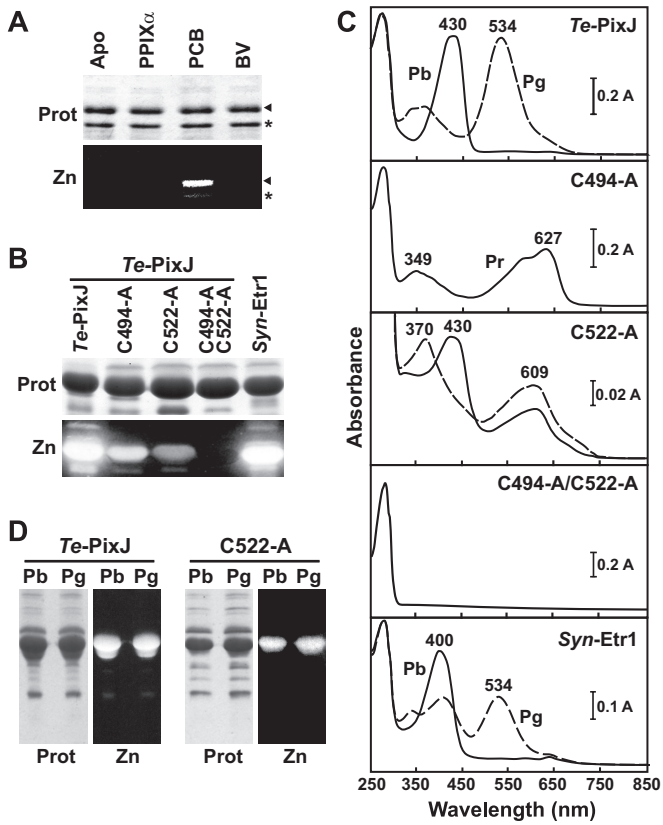

FIGURE 2. **Assembly of *Te*-PixJ and *Syn*-Etr1 with PCB.** *A*, *Te*-PixJ specifically binds PCB. *E. coli* extracts containing His_6-tagged wild-type *Te*-PixJ(Cyc-GAF) apoprotein were incubated with protoporphyrin IXα (*PPIX*α), BV, or PCB. The *Te*-PixJ(Cyc-GAF) polypeptide was then purified by Ni-NTA chromatography, subjected to SDS-PAGE, and either stained for protein with Coomassie Blue (*Prot*) or assayed for the bound bilin by zinc-induced fluorescence (*Zn*). *Apo*, apoprotein before incubation with the bilins. The *arrow* indicates the full-length *Te*-PixJ(Cyc-GAF) polypeptide, whereas the *asterisk* indicates a likely N-terminal degradation product that binds chromophore. *B*, covalent binding of PCB with wild-type *Syn*-Etr1(Cyc-GAF) and with *Te*-PixJ(Cyc-GAF) cysteine mutants affected in the bilin attachment sites. The apoproteins were co-expressed with the pair of enzymes needed to synthesize PCB and then purified by Ni-NTA chromatography. SDS-PAGE analyses were as described in *panel A*. *C*, absorption spectra of samples in *panel B* either kept in the dark (Pb and Pr, *solid lines*) or following saturating blue light (Pg, *dashed lines*). *D*, purified *Te*-PixJ(Cyc-GAF) and the C522A chromoprotein were either irradiated with blue light (430 nm) to convert to the green-absorbing state (Pg) or left in the dark-adapted blue-absorbing state (Pb). The samples were then heated in SDS-PAGE buffer and subjected to denaturing electrophoresis. The resultant SDS-PAGE gel was either stained for protein with Coomassie Blue (*Prot*) or assayed for the bound bilin by zinc-induced fluorescence under UV light (*Zn*).

C494A/C522A apoprotein failed to bind PCB covalently as judged by the lack of zinc-induced fluorescence and the lack of UV-visible absorption beyond 280 nm (Fig. 2, *B* and *C*).

Rockwell *et al.* (24) also identified a comparably positioned cysteine in the Cyc-GAF domain of a paralog of *Te*-PixJ, *T. elongatus* Tlr0924, as potentially forming a second binding site with the chromophore but proposed that this linkage was broken upon photoconversion from Pb to Pg. If true, we reasoned that the bilin bound to the C522A variant would lose its only covalent thioether linkage (provided by Cys-494) upon blue light exposure and thus readily dissociate from the apoprotein after denaturation under acidic conditions. To test this hypothesis, wild-type and C522A mutant chromoproteins were heated in SDS-PAGE buffer either before or after photoconversion with blue light and then examined for the amount of bilin

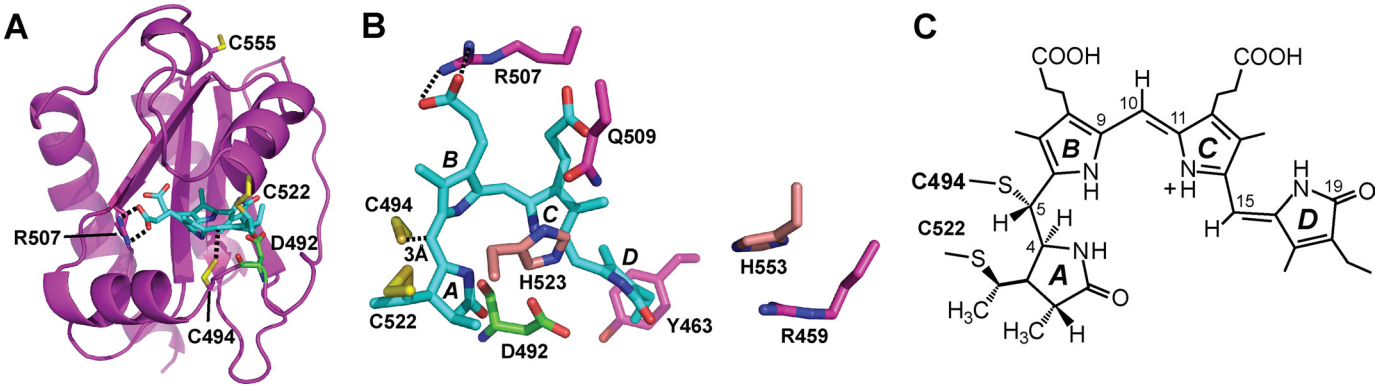

FIGURE 3. **Proposed three-dimensional structure of *Te*-PixJ(Cyc-GAF).** *A*, ribbon model of the structure based on alignment of *Te*-PixJ(Cyc-GAF) with *SyB*-Cph1(GAF) and threaded using SWISS-MODEL into the three-dimensional structure of *SyB*-Cph1(GAF) (PDB ID code 2K2N (8)). PCB is shown in *cyan*, the three *Te*-PixJ(GAF) cysteines (Cys-522, Cys-555, and Cys-494) are shown in *yellow*, Asp-492 is shown in *green*, and Arg-507 is shown in *magenta* with its potential salt bridges to the PCB B-ring propionate side chain indicated by the *dashed lines*. *B*, top view of the bilin and nearby amino acids. The A–D pyrrole rings are indicated. *C*, schematic representation of the proposed PVB-type chromophore linked via a double thioether linkage between Cys-494 and Cys-522 and the C5 and $C3^1$ carbons, respectively.

bound by zinc-induced fluorescence. As can be seen in Fig. 2*D*, the state of the photoreceptor had no obvious impact on bilin attachment, indicating that the Cys-494 linkage was equally stable in both spectral forms. Collectively our data point to both Cys-522 and Cys-494 binding the chromophore independently and indicate that the stability of the Cys-494 linkage is unaffected by the spectral form of the photoreceptor.

Molecular Modeling Points to Cys-494 Binding PCB via the C4=C5 Bridge—Under the assumption that Cys-494 also participates in PCB binding via a thioether linkage, we attempted to determine its linkage site to the chromophore. As a first step, we generated a homology model of *Te*-PixJ(Cyc-GAF) using as a template the three-dimensional solution structure of its closest available relative (*i.e.* the PAS-less Phy *SyB*-Cph1 (8)) in combination with our alignment of cyanochromes (Fig. 3*A*). The predicted chromophore pocket was similar to other Phys, including the appropriate placement of residues known to be key to Phy photochemistry (5, 8, 31, 42), confirming that the model represents a good reflection of the *Te*-PixJ(Cyc-GAF) structure, especially for conserved features (Fig. 3, *A* and *B*). When the predicted position of Cys-494 was examined specifically, we found that it could extend toward PCB but from the opposite side as Cys-522, and importantly, point toward the C4=C5 methine bridge (Fig. 3, *A* and *B*). Together with the prediction that PCB converts to a PVB-like adduct upon attachment (30), a likely scenario is that Cys-494 spontaneously attacks the C4=C5 bond to form a thioether linkage with either the C4 or the C5 carbon, which then generates a PVB-type chromophore (Fig. 3*C*). The C5 carbon is the more likely target given its closer predicted distance (3.05 Å *versus* 4.28 Å) to the Cys-494 sulfhydryl group.

For further support of a double thioether linkage of *Te*-PixJ to a PVB-type chromophore, we compared the absorption spectra of wild-type *Te*-PixJ(Cyc-GAF) with the C494A and C522A chromoproteins after denaturation in acidic urea, which can better distinguish between PCB and PVB due to reduced modification of bilin photoabsorption by non-covalent contacts with the apoprotein. As reported previously (30), wild-type *Te*-PixJ(Cyc-GAF) has two absorption maxima at 564 and 597 nm as Pb in acidic urea with the denatured chromoprotein being poorly photochromic after blue light irradiation (Fig. 4). Denatured Pg has a maximal absorption at 541 nm, which is then red-shifted by blue light, suggesting that the bilin in Pg retains some ability to photoisomerize back to the Pb geometry without non-covalent protein contacts. In agreement with a PVB-type chromophore, these spectra were substantially blue-shifted by 50–70 nm as compared with the Pr and Pfr forms of *SyB*-Cph1(GAF), which bears a PCB chromophore linked via a single thioether linkage to the $C3^1$ carbon (8) (Fig. 4).

We predicted that elimination of the Cys-494 thioether linkage in *Te*-PixJ(Cyc-GAF) should now generate a PCB-type chromophore attached by a single thioether linkage between Cys-522 and the $C3^1$ carbon. In agreement, the absorption spectrum of the non-photochromic C494A mutant in acidic urea was identical to that of *SyB*-Cph1(GAF) denatured as Pr (Fig. 4). Both spectra were slightly blue-shifted relative to free PCB (maximum absorbance of ~687 nm), implying that the bilin in *Te*-PixJ(Cyc-GAF) remained bound to the Cyc-GAF domain (Fig. 4). Similar analysis of the C522A mutant denatured as Pb, which we predicted would bind PCB via a thioether linkage at the C4 or C5 position to generate a PVB-type chromophore, did not initially generate the expected PVB spectra in acidic urea. Instead, its absorption spectrum closely matched that of free PCB (Fig. 4 and supplemental Fig. 3*A*), suggesting that the chromophore was released from Pb in acidic urea. However, analysis of the Pg form of the C522A mutant after photoconversion implied that the chromophore remained bound. Its absorption in acidic urea was substantially blue-shifted from free PCB and remained photochromic, a property not observed with free PCB (Fig. 4).

To further explore the stability of the bilin linkage between Cys-494 and the chromophore, we first dissolved the assembled C522A mutant in acidic urea as Pb or Pg, precipitated the chromoprotein with trichloroacetic acid, and then measured the absorption of the soluble and precipitated fractions (supplemental Fig. 3). As observed above, the precipitated forms of Pb and Pg retained a near equal amount of chromophore following SDS-PAGE with about 50% released into the soluble fraction, indicating that the linkage of the bilin to Cys-494 was equally stable in both spectral forms. The bound forms had absorption spectra similar to PVB (absorption maximum at 611 nm). The released form from Pg had a similar absorption, which likely

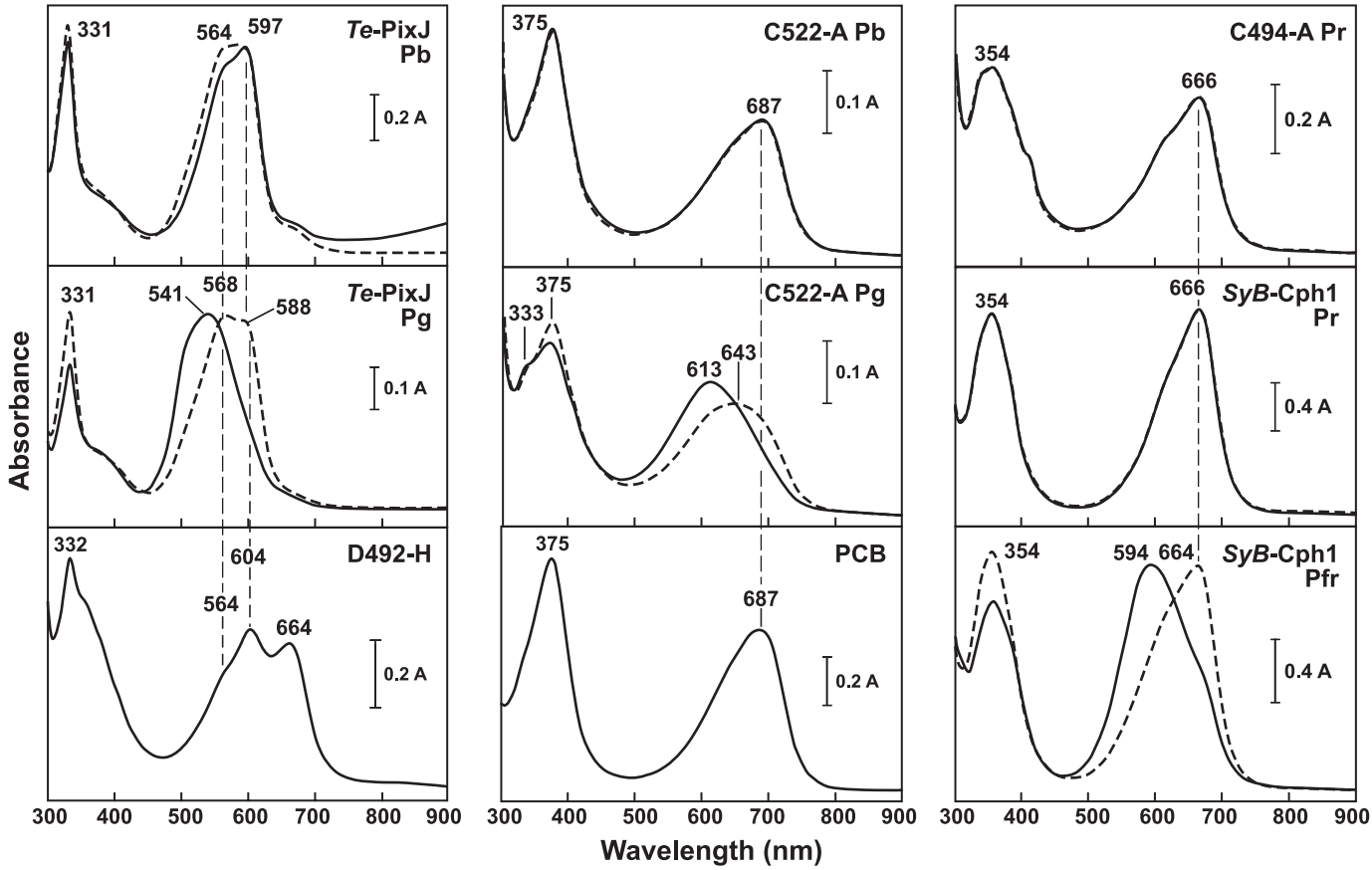

FIGURE 4. **Absorption spectra of *Te*-PixJ(GAF) variants under denaturing conditions.** Purified *Te*-PixJ(Cyc-GAF), the D492H, C494A, and C522A mutants, and wild-type *SyB*-Cph1(GAF) were assembled with PCB and then denatured in acidic urea in either their dark-adapted states (Pb for *Te*-PixJ and Pr for *SyB*-Cph1) or their excited states (Pg for *Te*-PixJ and Pfr for *SyB*-Cph1). UV-visible absorption spectra were measured either in darkness (*solid lines*) or following irradiations with light near their peak absorption (*dashed lines*). Free PCB was included for comparison. Absorption maxima are indicated.

represents free PVB. However, the released form from Pb had a red-shifted absorption spectrum, which could reflect either photoisomerized free PVB or release of a non-covalently bound PCB-type bilin (absorption maximum at 694 nm).

NMR Spectroscopy of the Te-PixJ Chromophore in Pg and Pb States—To help define the chemistry and architecture of the bilin during photoconversion, we examined by NMR *Te*-PixJ-(Cyc-GAF) assembled with isotopically labeled PCB. Using our previously described labeling scheme with [^{15}N]ALA and 5-[^{13}C]ALA (8, 31), we selectively introduced ^{15}N into all four pyrrole ring nitrogens or ^{13}C into the C4, C5, C9, C10, C11, C15, and C19 carbons of the chromophore (Fig. 5*A*). Data from the ^{1}H-^{15}N two-dimensional correlation revealed five distinct ^{15}N chemical shifts of 127.50, 131.25, 132.25, 132.40, and 145.00 ppm, representing the four pyrrole amides (Fig. 5*B*). These data unambiguously demonstrate that all four nitrogens are protonated in Pb, with the smaller split peaks at ~132+ ppm most likely reflecting a single N–H moiety experiencing minor conformational exchange between two distinct states. These data were in stark contrast to [^{15}N]PCB *SyB*-Cph1(GAF) where only one N–H group (D ring) was detected in Pr, most likely because signals from the other three pyrrole nitrogens (rings A, B, and C) were lost due to solvent exchange (31).

Upon photoconversion to Pg, all four N–H peaks remained evident with the 132+ peaks appearing to merge into a single more intense peak with a chemical shift at 132.25, demonstrating unambiguously that the Pg state is fully protonated as well (Fig. 5*B*). Of the four pyrrole nitrogens, only the ^{1}H-^{15}N cross-peak at 9/145 ppm experienced a dramatic change in chemical shift, most likely moving to the 10.3/135 coordinates (Fig. 5*B*). This simultaneous ^{1}H chemical shift increase (or deshielding) and ^{15}N decrease (or shielding) during the Pb to Pg photoconversion could result from either a change in the hydrogen bonding of this nitrogen or a strong geometric strain. Taken together, it appears that: (i) the protonated pyrrole nitrogens in the Cyc-GAF domain are fully protected from the solvent in both conformers (Pb and Pg), (ii) the Pg chromophore is more stable/homogenous than Pb, and (iii) only one of the N–H moieties experiences a significant change in its chemical environment during photoconversion.

Labeling the chromophore with 5-[^{13}C]ALA allowed us to examine the environment of the methine bridges between the pyrrole rings and the D-ring carbonyl during Pb → Pg photoconversion (14) (Fig. 5*A*). Combined one-dimensional (by ^{13}C direct detection) and two-dimensional (^{1}H-^{13}C HSQC) NMR detected distinct ^{13}C peaks at 108.25 and 108.75 ppm and a cluster at 110 ppm within the methine region (Fig. 5*C*). The cluster at 110 ppm clearly represented a single C–H group experiencing either a shifting proton or slight changes in geometry, as evidenced by the single ^{13}C peak seen in the one-dimensional spectrum and the heterogeneity in the ^{1}H dimension of our ^{1}H-^{13}C HSQC plot. The peaks at 108.25 and 108.75 ppm

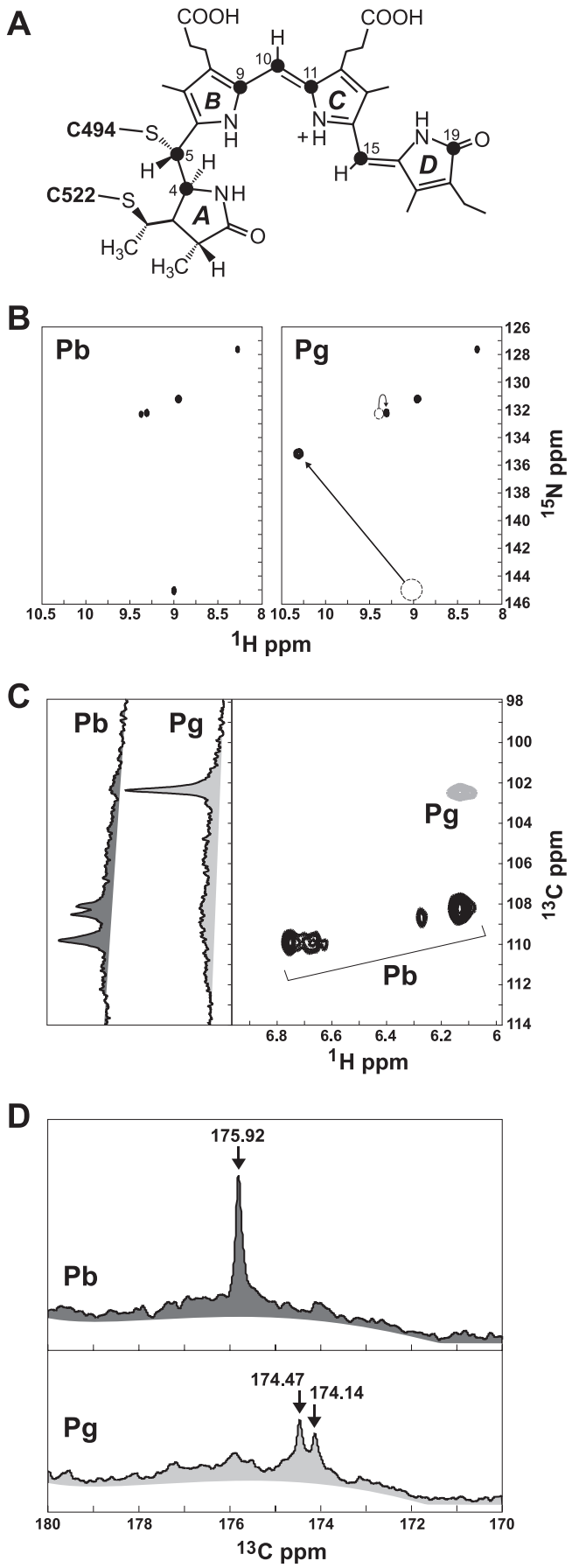

could reflect either a single C–H moiety experiencing conformational exchange or two distinct methine groups. In the latter case, the less intense peaks might have a reduced signal in the two-dimensional plot from solvent exchange. Although we cannot yet assign these peaks to specific methine carbons (C4, C5, C10, and C15), the ^{13}C NMR spectrum detected at least two for Pb. Strikingly, upon photoconversion to Pg, all these peaks disappeared, and an intense singlet emerged at 102.5 ppm (Fig. 5*C*), suggesting that substantial changes occur in or around the three bridges. Because we assume that the B–C and C–D methine bridges in PVB remain intact to generate the required extended π-conjugation system, conformational exchange likely explains the loss of these peaks.

When the C=O region of the ^{13}C direct detect spectrum was analyzed, which would measure the environment of the C19 carbonyl of the D ring, we found a single peak at 175.92 ppm for Pb. Its sharpness implies that the D-ring is held rigidly in this state, most likely via hydrogen bonds (Fig. 5*D*). Upon photoconversion to Pg, this peak moved ~2 ppm and split into a less intense doublet (174.47 and 174.14 ppm), indicating conformational exchange/motion between two closely related yet distinct geometries (Fig. 5*D*). Conformational exchange for the D-ring carbonyl combined with environmental changes surrounding a single pyrrole N–H point to movement in and around the D ring during Pb → Pg photoconversion. This motion could reflect the proposed *Z* to *E* rotation around the C15=C16 bond of the bilin, changes in the immediate chemical environment of the D-ring, or formation or loss of hydrogen bond(s) during Pg formation (*e.g.* with the His-553 side chain (Fig. 3*B*)) (4, 5, 8).

NMR Spectroscopy Reveals Global Light-induced Movements of Te-PixJ(GAF)—To study the global movements of the *Te*-PixJ(Cyc-GAF) protein moiety during photoconversion, we examined by two-dimensional NMR the holoprotein isotopically labeled with ^{15}N. ^{15}N was uniformly incorporated by expressing the recombinant polypeptide in minimal medium containing $^{15}NH_4Cl$ as the main nitrogen source along with excess non-labeled ALA to minimize bilin labeling. Our initial analysis with wild-type protein assembled with PCB generated poorly resolved ^{1}H-^{15}N HSQC spectra consistent with the possible presence of multiple states caused by oligomerization (data not shown). One possible culprit was Cys-555, which was predicted from the three-dimensional model to be solvent-exposed and thus could form an intermolecular disulfide bridge (Fig. 3*A*). To avoid this potential complication, we generated a C555A mutant of *Te*-PixJ(Cyc-GAF). This mutant retained its ability to assemble with PCB and had normal Pb and Pg absorp-

FIGURE 5. **NMR spectroscopy of *Te*-PixJ(Cyc-GAF) assembled with [^{15}N]PCB or [^{13}C]PCB.** *A*, proposed structure of PVB bound via Cys-494 and Cys-522. The *filled circles* locate the carbons labeled with ^{13}C. *B*, two-dimensional ^{1}H-^{15}N HSQC NMR spectra of [^{15}N]PCB-labeled *Te*-PixJ(GAF) before (Pb) and after (Pg) irradiation with saturating blue light. The *arrows* highlight the ^{15}N chemical shifts that change position upon Pb → Pg photoconversion. *C*, one-dimensional ^{13}C and two-dimensional ^{1}H-^{13}C NMR spectra of [^{13}C]PCB-labeled *Te*-PixJ(Cyc-GAF) in the methine region of the spectra before (Pb) and after (Pg) irradiation with saturating blue light. *D*, one-dimensional ^{13}C NMR spectra of [^{13}C]PCB-labeled *Te*-PixJ(Cyc-GAF) before (Pb) and after (Pg) irradiation with saturating blue light in the C=O region of the spectra (170–180 ppm).

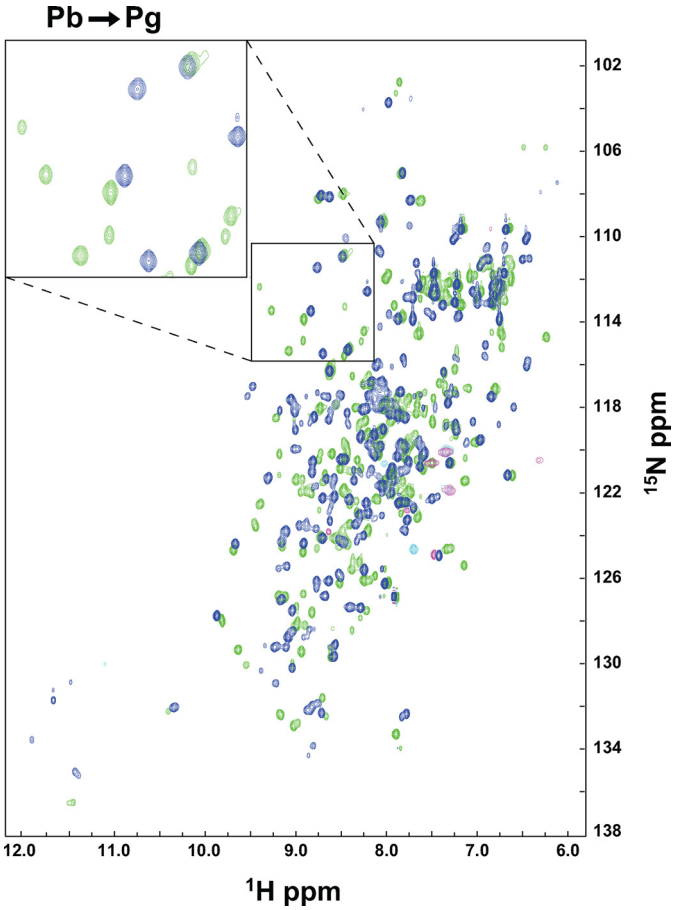

FIGURE 6. **Two-dimensional ^{1}H-^{15}N HSQC NMR spectra of [^{15}N]*Te*-PixJ-(Cyc-GAF) in the Pb and Pg states.** NMR data were collected with the C555A variant of *Te*-PixJ(Cyc-GAF) with the polypeptide uniformly labeled with ^{15}N and assembled with unlabeled PCB. *Blue*, NMR spectrum of Pb. *Green*, NMR spectrum of Pg. *Magenta*, anti-alias chemical shifts. The *inset* shows a magnification of a region in the ^{1}H-^{15}N HSQC spectra that includes a number of peaks that substantially change position upon Pb to Pg photoconversion.

tion spectra. Importantly, it also provided highly resolved ^{1}H-^{15}N HSQC spectra with uniformly sharp peaks, suggesting that this mutant remains monomeric even at high protein concentrations (Fig. 6 and data not shown). The number of peaks in the ^{1}H-^{15}N HSQC spectrum for Pb closely matched the predicted number of backbone and side chain N–H resonances in this 177-amino acid chromoprotein.

When photoconverted to Pg by blue light, the C555A mutant of [^{15}N]*Te*-PixJ(Cyc-GAF) generated a markedly different ^{1}H-^{15}N HSQC spectrum (Fig. 6). Close inspection revealed appreciable chemical shifts (reflecting chemical and magnetic environmental changes) for ~50% of the residues, indicating that the GAF domain of *Te*-PixJ may experience numerous conformational changes in its backbone, side chain, and secondary structure upon photoconversion. Some smaller secondary peaks were also observed that could reflect minor subspecies or multiple stable conformations for several amide groups. Many of the chemical shifts present in Pb were completely absent in Pg (Fig. 6). Taken together with their non-overlapping absorption spectra in the blue/green spectral region for Pb and Pg (Fig. 2*B*), it appears that *Te*-PixJ(Cyc-GAF) contains little residual Pb upon photoconversion to Pg, unlike canonical Phys, which can contain upwards of 25% Pr contamination when saturating red light is used to generate Pfr (49). Moreover, the ^{1}H-^{15}N HSQC peaks lost upon photoconversion to Pg did not return even after a 3-month incubation in darkness at 25 °C (data not shown), indicating that the Pg form of *Te*-PixJ is remarkably stable against thermal reversion.

IR and Resonance Raman Spectroscopic Support for a PVB Chromophore—To provide further support for a PVB-type bilin in *Te*-PixJ(Cyc-GAF), we employed both IR and RR spectroscopy and compared these spectra with those calculated for *in vacuo* model bilins. We restricted our *in vacuo* models to several derivatives of PCB that represented the range of likely candidates for the bound chromophore (24, 30). These included: PCB with and without a second thioether linkage at C10, PVB with or without a second thioether linkage at C4 or C5, phycourobilin (PUB) with a second thioether linkage at C4 or C5, and phycoerythrobilin (PEB) with a second thioether linkage at C15. In all cases, the C3 ethylidene group was replaced with an ethyl to mimic the thioether linkage to Cys-522. Except for PCB-B and -C, which lack the proton at the ring B and C nitrogens, respectively, the chromophores were modeled as fully protonated. In addition, chromoproteins assembled with [^{13}C]-labeled PCB at the C4, C5, C9, C10, C11, C15, and C19 carbons (Fig. 5*A*) were used for the RR and IR analyses to support the vibrational assignments. For IR spectroscopy, we generated a Pg-Pb difference spectrum to minimize signals from the protein moiety. From these analyses, we tried to identify candidate bilins for which the calculated spectra reproduced the main features of the experimental spectra, rather than seeking perfect agreement for the position of individual bands.

The experimental IR difference spectrum of *Te*-PixJ(Cyc-GAF) had a number of positive and negative peaks between 1500 and 1700 cm^{-1} that included chromophore bands as well as amide-I bands from the protein (Fig. 7*A* and supplemental Fig. 4*B*). Several of these peaks matched calculated IR spectra for a variety of PCB derivatives with the best fit being the PVB modified at either the C4 or the C5 carbon. A surprisingly poor fit was evident for PCB modified at the C10 carbon, contradicting the proposal that this site links the bilin (24). The calculated spectrum for PCB-C10 predicted prominent peaks only above 1700 cm^{-1}, which contain the stretching modes of the propionate side chain C=O groups of the bilin (Fig. 7*A* and supplemental Fig. 5*B*). These peaks were absent in the experimental data, suggesting either that Pb → Pg photoconversion does not drastically perturb these carboxyl groups or that they form salt bridges with the Cyc-GAF domain, thus moving the respective C=O stretching modes out of this spectral region.

RR spectroscopy of *Te*-PixJ(Cyc-GAF) was performed in H_2O and D_2O buffers to determine the protonation state of the bilin by the presence or absence of the characteristic N–H in-plane bending mode at ~1570 cm^{-1}, which downshifts by ~500 cm^{-1} upon H/D exchange (Fig. 7*C*). The RR spectra of *Te*-PixJ(Cyc-GAF) as Pb and Pg displayed vibrational band patterns similar to canonical Phys, with the most prominent bands above 1600 cm^{-1} readily attributable to modes dominated by C=C stretching coordinates (Fig. 7*C* and supplemental Fig. 4*A*). Among the calculated RR spectra, the best fit to the exper-

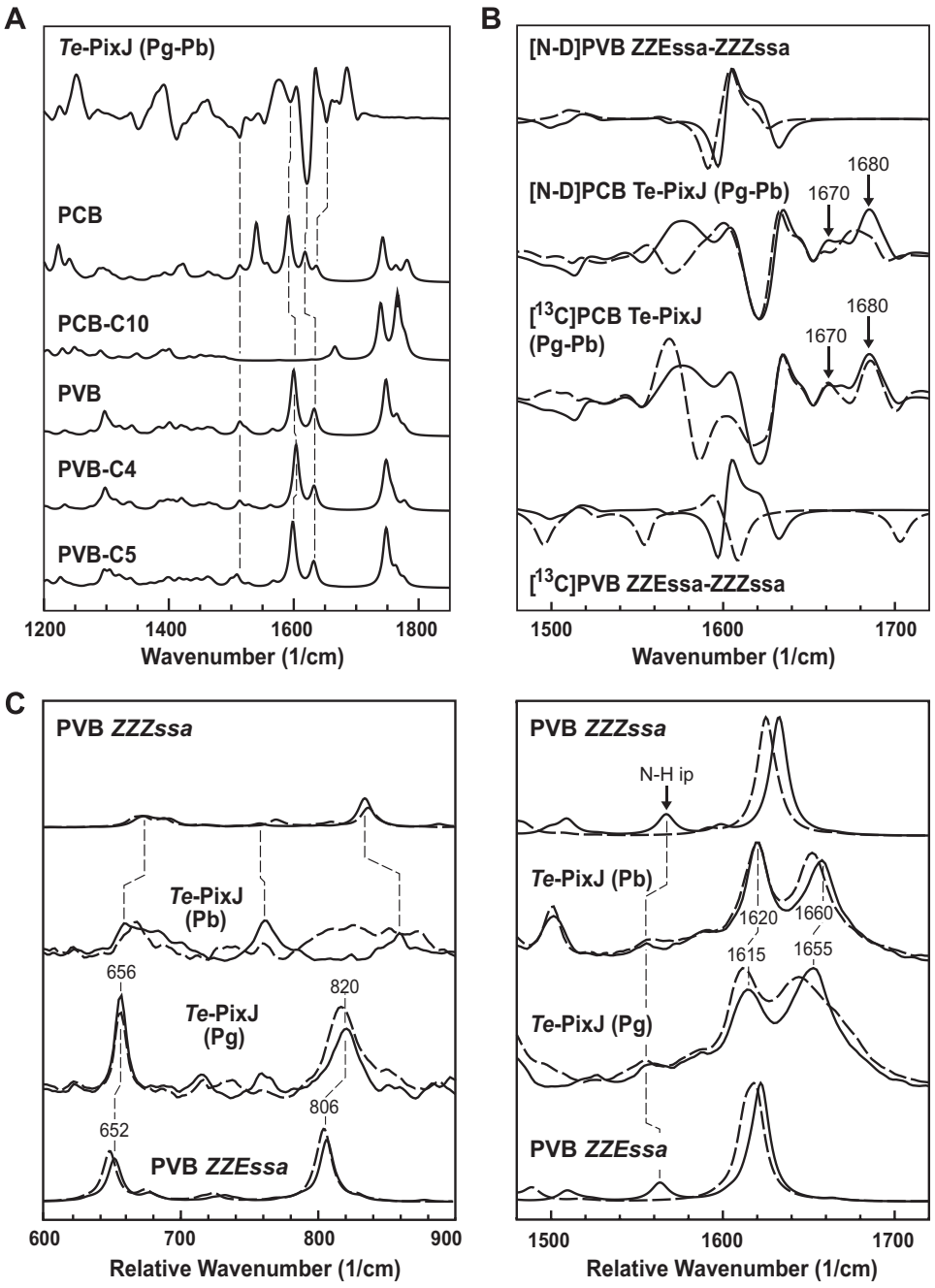

FIGURE 7. **IR and RR spectroscopy of *Te*-PixJ(Cyc-GAF).** *A*, experimental Pg-Pb difference IR spectra as compared with calculated IR spectra for various chromophore variants. *PVB-C4*, *PVB-C5*, and *PCB-C10* denote PVB and PCB variants bound via the C4, C5, and C10 carbons, respectively. *B*, experimental Pg-Pb and calculated (*ZZEssa-ZZZssa*) IR difference spectra for chromophores with protonated (*solid line*) and deuterated (*dashed line*) pyrrole nitrogens (*top two spectra*) and for the natural abundance (*solid line*) and the ^{13}C-labeled (*dashed line*) chromophores (*bottom two spectra*). For the location of the ^{13}C-labeled carbons, see Fig. 5*A*. *Solid lines* = H_2O or ^{12}C samples. The calculated spectra refer to the PVB chromophore. *C*, experimental RR spectra of the Pb and Pg states as compared with calculated RR spectra of PVB in the *ZZZssa* and *ZZEssa* geometries. *Solid* and *dashed lines* refer to chromophores protonated and deuterated at the pyrrole nitrogens, respectively.

imental data were found for PCB and PVB, which have strong bands in this region as compared with PUB and PEB. For example, the strongest RR band for PUB was predicted to be at ~1300 cm^{-1} (supplemental Fig. 4*A*). Due to the saturation of the A–B and C–D methine bridges of PUB, one would expect the C=C stretching region of the RR spectrum to be dominated by the modes localized in the central dipyrrolic unit. In fact, the calculated RR spectrum for PUB is similar to the calculated and experimental RR spectra for hexamethylpyrromethene (50).

As evidence against a PEB-like chromophore, the experimental RR spectrum of the ^{13}C-labeled sample displayed isotopic shifts that are clearly better matched by the calculated 30 cm^{-1} downshift of the prominent 1622/1633 cm^{-1} band of a PVB chromophore rather than the substantially larger 50 cm^{-1} downshift predicted for PEB (supplemental Fig. 5*A*). This difference is due to the different labeling patterns of the A–B and C–D methine bridges where the most intense C=C stretching bands in PEB and PVB are located, respectively. Residual intensities at 1660 cm^{-1} are readily attributed to amide-I bands.

Finally, the RR calculations for various PCB, PEB, and PVB species predict three or four modes between 1600 and 1660 cm^{-1}, which mainly include the C=C stretching coordinates of ring D and the A–B and C–D methine bridges. At first glance, none of these calculated spectra satisfactorily fit the two-banded pattern at 1620 and 1658 cm^{-1} in the experimental spectra (Fig. 7*C*). However, if we take into account: (i) that a considerable contribution to the 1660 cm^{-1} peaks originates from the Raman band envelope of the amide I and (ii) that structural distortions of the bilin with respect to the *in vacuo* geometry may cause a redistribution of the internal coordinates among the modes in this region, it is possible that the C–D methine bridge stretching, which is known to provide the largest contribution to the RR signal, may be divided into two modes when bound to the protein instead of one modeled *in vacuo*.

Absorption spectra predicted that the chromophore of the C494A mutant of *Te*-PixJ(Cyc-GAF) is PCB rather than PVB in wild type. RR spectra of the mutant confirmed this expectation (supplemental Fig. 2*B*). Only a single band was observed for the C494A mutant, which was similar to that generated for *SyB*-Cph1 and *Syn*-Cph1 shown previously to bind PCB via a single thioether linkage involving the C3^1 carbon (8, 31). Accordingly, the IR

and RR spectra favor PVB as the chromophore in wild-type *Te*-PixJ.

ZZZssa and ZZEssa Geometries Are Predicted for Pb and Pg, Respectively—Although the experimental IR and RR spectra support a PVB-like chromophore in both the Pb and the Pg states (Fig. 7 and supplemental Fig. 5), calculated spectra fail to distinguish between a thioether attachment to the C5 or C4 atom or just the addition of a hydrogen at either position. Moreover, it remains to be explained how PVB can undergo such a substantial red shift of its absorption (~106 nm) during the Pb → Pg conversion. It is conceivable, for example, that *Z*/*E* photoisomerization of the B–C methine bridge could occur simultaneous with photoisomerization of the C–D methine bridge. However, such a scenario can be ruled out by our NMR analyses, which showed that only one N–H group is active during photoconversion (Fig. 5*B*). Thus, the absorption changes of *Te*-PixJ(Cyc-GAF) upon photoconversion are likely to be ascribed to differentially twisted methine bridge conformations tuning the extended π-conjugation system.

In the experimental RR spectra, the two prominent bands in the C=C stretching region shifted down by ~5 cm^{-1} upon conversion from Pb to Pg (Fig. 7*C*). These downshifts were very similar to those predicted upon transition from *ZZZssa* to *ZZEssa* and agreed well with experimental analyses of biliproteins containing PVB (51). However, the intensities of the bands in this region were not well reproduced, even taking into account a contribution from the broad amide-I band to the highest frequency mode at 1660 cm^{-1} (Fig. 7*C*). The analysis of the N–H bending modes and the H/D isotopic shifts in these spectra suggested that hydrogen-bond interactions of the N–H groups of the rings B and C cause this discrepancy. First, the characteristic in-phase N–H bending, which was seen as a prominent peak between 1550 and 1590 cm^{-1} for the calculated *ZZZssa* and *ZZEssa* geometries of protonated bilins, was weak in the experimental spectra of Pb and Pg (Fig. 7*C*). Second and paralleling our NMR data (Fig. 5*B*), the C=C stretching at 1620 (Pb) and 1615 cm^{-1} (Pg) was nearly insensitive toward H/D exchange, again unlike the calculations for protonated bilins. Conversely, the IR difference spectrum (Pg minus Pb) in the N–H out-of-phase in-plane bending (1510–1530 cm^{-1}) was satisfactorily reproduced by the calculated *ZZEssa-ZZZssa* difference spectrum (Fig. 7*B*).

Cognizant of the limitations of *in vacuo* spectra, the $^{13}C/^{12}C$ isotopic shifts in the RR and IR spectra were largely consistent with the assignment of the Pb and the Pg chromophores as PVB in a *ZZZssa* and *ZZEssa* configuration, respectively (supplemental Fig. 5*A*). In the spectral region between 600 and 850 cm^{-1}, the bands for Pb were relatively weak such that only three features could be identified that were consistent with the predictions for the *ZZZssa* geometry (Fig. 7*C*). In Pg, however, this region was dominated by two bands of medium RR intensity at 656 and 820 cm^{-1}, which agreed with the calculated modes at 652 and 806 cm^{-1}, respectively (Fig. 7*C*). For these modes, with the latter one (806 cm^{-1}) being dominated by the C–H out-of-plane coordinates of the C–D methine bridge, the calculated D/H and $^{13}C/^{12}C$ isotopic shifts agreed well with the experimental RR data (Fig. 7*C* and supplemental Fig. 5*A*).

The IR difference spectra do not reveal changes in the configuration of the C–D methine bridge but can provide complementary information about protein structural changes associated with the Pb → Pg transition. The positive and negative signals at 1680 and 1670 cm^{-1} shown in Fig. 7, *A* and *B*, could be attributed to a change of the amide I bands in view of its insensitivity toward $^{13}C/^{12}C$ substitution. The height of the difference signal relative to the absolute intensity suggests that only a few peptide bonds in the polypeptide backbone undergo a light-induced conformational change. Thus, Pb to Pg phototransformation may be associated mainly with changes in amino acid side chain conformations.

Te-PixJ Mutagenesis Yields Insights into Cyanochrome Function—To assess the contributions of residues conserved within cyanochromes, we examined the photochemical impact of several in *Te*-PixJ(Cyc-GAF) by site-directed mutagenesis. For example, Asp-492 lies within the conserved DPCF motif unique to cyanochromes. Based on its predicted position near the chromophore, it may have an analogous function to the aspartic acid in the DIP domain of canonical Phys, which plays a key role in the deprotonation/protonation cycle of the bilin by helping form the hydrogen-bond network between the bilin and the pyrrole water (4, 42, 43) (Fig. 1*B*). D492A, D492H, and D492N variants all bound PCB as judged by zinc-induced fluorescence of the chromoprotein following SDS-PAGE (Fig. 8*A*). However, instead of forming Pb, they generated a substantially red-shifted pigment with an absorption maximum at 562 nm (Fig. 8*B*). The mutant chromoproteins were also photochemically locked during green light irradiation and were intensely fluorescent with excitation and emission maxima at 552 and 578 nm, respectively (Fig. 8*C*), indicating that Asp-492 is critical for proper cyanochrome photochemistry. Spectral analysis of denatured D492H chromoprotein suggests that these mutants contain a mixture of bound PVB- and PCB-type chromophores (Fig. 4).

The thioether linkage to the $C3^1$ carbon is also important for photochemistry. In addition to impaired bilin binding and aberrant photoconversion, the C522A mutant was strongly fluorescent with 525 and 577 nm excitation and emission maxima, respectively (Fig. 8*C*). Our Cys-494 *Te*-PixJ(GAF) substitutions, which removed the second bilin attachment site, were also strongly fluorescent but were substantially red-shifted as compared with the Cys-522 mutants (excitation and emission maxima at ~620 and 650 nm, respectively (Fig. 8*C* and supplemental Fig. 2). The absorbance, fluorescence, and RR spectra of these Cys-494 mutants were almost identical to comparable mutants in the PAS-less Phy *Sy*B-Cph1 (31) and had similar fluorescence properties to mutants affecting the Cyc-GAF domain of the *Te*-PixJ relative, Tlr0924 (24).

Two conserved arginines that interact with the propionic acid side chains of the bilin were previously shown to be important for photochemistry and Pfr stability of *Deinococcus radiodurans* BphP and *SyB*-Cph1 (Arg-133 and Arg-101 in *SyB*-Cph1) (8, 42). In cyanochromes, Arg-133 has been generally replaced by an alanine (Ala-518 in *Te*-PixJ), whereas Arg-101 has been replaced by a glutamine (Gln-509), indicating that the interaction of the protein with the bilin propionates is different in cyanochromes. In support, the Q509A mutant of *Te*-PixJ-

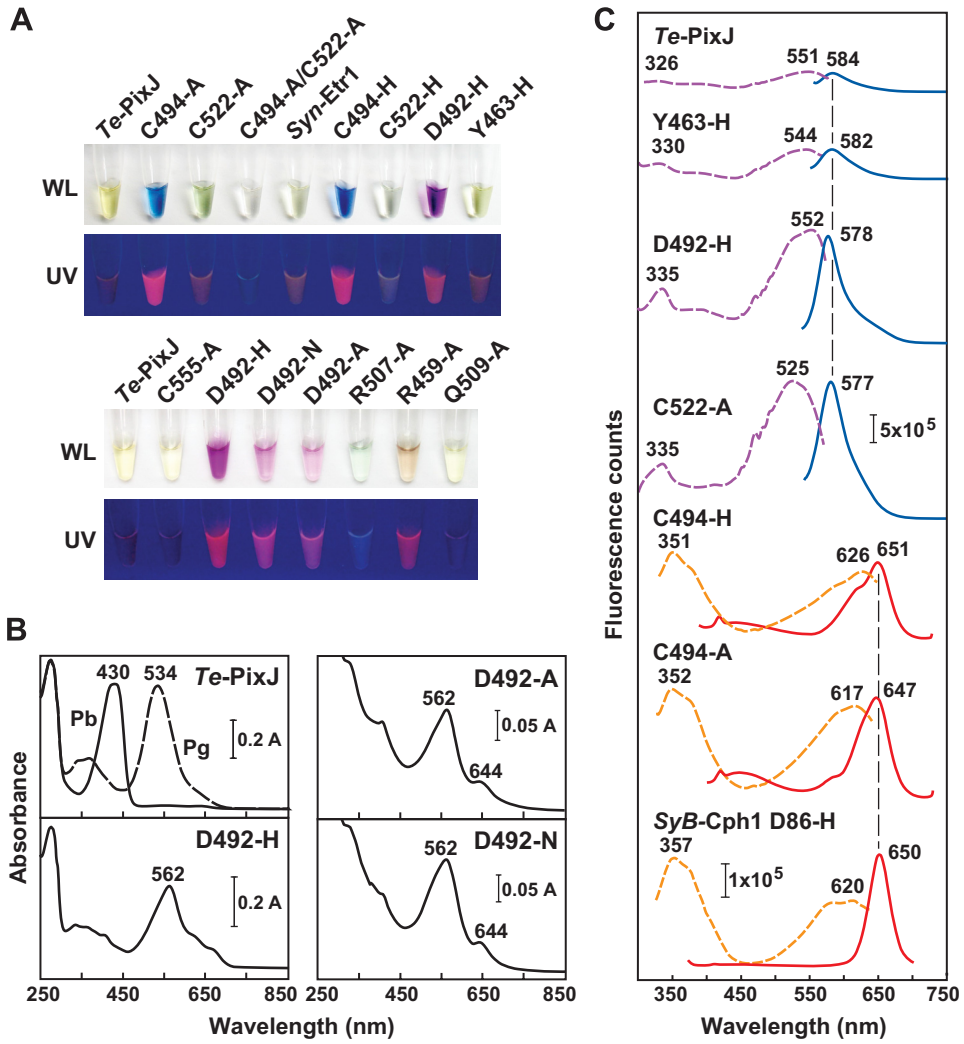

FIGURE 8. **Absorption and fluorescence properties of *Te*-PixJ(Cyc-GAF) mutants.** *A*, photographs of purified solutions of *Te*-PixJ(Cyc-GAF) and the mutants in white light (*WL*) or during irradiation with UV light. Samples were kept in the dark prior to photography. *Syn*-Etr1(Cyc-GAF) is included for comparison. *B*, absorption spectra of the *Te*-PixJ(Cyc-GAF) mutants affecting Asp-492. *C*, fluorescence excitation (*dashed lines*) and emission spectra (*solid lines*) of a subset of *Te*-PixJ(Cyc-GAF) variants shown in *panel A*. Excitation and emission maxima are indicated. The fluorescence spectra of the D86H mutant of *SyB*-Cph1(GAF) are included for comparison.

(Cyc-GAF) bound PCB and was photochemically indistinguishable from wild type (supplemental Fig. 6). However, we noticed that Arg-507 might provide a substitute connection to the B-ring propionate; it is conserved among cyanochromes but not among canonical Phys and is present two residues upstream from Gln-509. The R507A variant assembled with PCB but less efficiently than wild type (supplemental Fig. 6*A*). The resulting chromoprotein had a substantially altered and weak absorption in the visible region with a maximum at 643 nm and was not photochromic in blue or red light (supplemental Fig. 6*B*). Taken together, it appears that the predicted double salt bridge between Arg-507 and the B ring propionate is critical for the proper photochemistry of *Te*-PixJ as its counterpart is for canonical Phys (8, 42). However, unlike many photochemically impaired mutants, the R507A chromoprotein was poorly fluorescent (Fig. 8*A*).

Lastly, we substituted Tyr-463 and Arg-459 that are highly conserved within the Phy superfamily and important for Pr → Pfr photoconversion for some (42, 52, 53) but not all Phy clades (31). A Y463H variant bound PCB well and generated Pb but photoconverted to a bleached, slightly fluorescent form in blue light (supplemental Fig. 6). The bleached Pg form of Y463A failed to photoconvert back to Pb with green light. A R459A variant also bound PCB well (supplemental Fig. 6*A*). The ground Pb-like state had an absorption maximum at 415 nm, with additional peaks at 561 and 641 nm. When irradiated with blue light, these peaks converged to generate a relatively normal Pg absorption spectrum with a maximum at 531 nm (supplemental Fig. 6*B*). Additionally, the R459A mutant was fluorescent with excitation and emission spectra similar to C522A (Fig. 8*A* and data not shown). From these data, we can infer that Arg-459 is partially responsible for generating the Pb state but is not necessary for Pb → Pg photoconversion and stabilization of the Pg photoproduct.

The Synechocystis Ethylene Receptor Is a Cyanochrome—One novel member of the cyanochrome clade is *Synechocystis* sp. PCC6803 Etr1 (locus *slr1212*), which was previously shown to bind the gaseous hormone ethylene via its transmembrane receptor domain (40). Its Cyc-GAF domain contains all the conserved motifs found in the cyanochrome family including Cys-561 that could bind PCB via the $C3^1$ position and a second cysteine in the ETCF motif (Cys-533) that could provide a second docking site to the C4/5 position (Fig. 1*B*). When expressed recombinantly, we found that the Cyc-GAF domain of *Syn*-Etr1 readily bound PCB as determined by zinc-induced fluorescence of the chromoprotein following SDS-PAGE (Fig. 2*B*). The resulting biliprotein photointerconverted between Pb and Pg states with absorption maxima at 400 and 534 nm, respectively (Fig. 2*C*). This bilin ligase activity implies that *Syn*-Etr1 can act both as an ethylene receptor and as a light receptor.

DISCUSSION

Biochemical and phylogenetic analyses indicate that the cyanochromes represent a novel clade of Phy-type photoreceptors that predominately respond to blue and green light. By applying a combination of molecular modeling, biochemistry, and various spectroscopic methods to a representative, *Te*-PixJ, we provide evidence that cyanochromes are structurally similar to canonical Phys but that they bind the bilin via a unique architecture using two stable thioether linkages.

The first binding site is presumed to be identical to that of canonical Phys, which binds the bilin via a thioether bond between a positionally conserved cysteine (Cys-522 in *Te*-PixJ) and the C3^1 carbon of the A-ring ethylidene side chain. Like Rockwell *et al.* (24), we found a second binding site involving a second cysteine in a conserved DPCF motif. Although they proposed that the second cysteine binds to the C10 carbon of PCB to generate a rubin-like adduct that disengages upon photoconversion of Pb to Pg (24), our data are more consistent with PCB binding via the C4/C5 carbon to generate a PVB-like adduct that remains stable as both Pb and Pg. Ishizuka *et al.* (30) also proposed a PVB-type chromophore for these cyanochromes but speculated that reduction of the C4=C5 double bond occurred upon PCB binding by an intrinsic autoisomerase activity that moved this double bond to the C2/C3 position. Based on our data, the substantially blue-shifted absorption spectra of cyanochromes is explained by a shorter π-conjugation system, resulting from reduction of the A–B methine bridge during attachment of PCB to the second site at Cys-494. Once bound, the PVB chromophore for *Te*-PixJ(GAF) is protonated (cationic) in both the Pb and the Pg states similar to previous observations for the Pr and Pfr forms of canonical Phys (31, 54).

We note that several Phy sequences from cyanobacteria cluster phylogenetically within the cyanochrome family but are without the second cysteine, including members of the *Fremyella diplosiphon* RcaE subgroup (55) and possibly a PixJ relative from *Anabena* (*Nostoc*) sp. PCC7120 (Fig. 1*B*, supplemental Fig. 1, and supplemental Table 2). Spectroscopic studies of assembled *An(Nos)*-PixJ recently demonstrated that it photointerconverts between green- and red light- absorbing forms (25), indicating that it has distinct photochemical properties consistent with a different bilin linkage as compared with members of the cyanochrome clade. Consequently, these proteins may represent another photochemically distinct group of chromoproteins within the Phy superfamily.

Assembly studies with Cys-522 and Cys-494 mutants indicate that *Te*-PixJ can bind PCB by either thioether linkage independently, albeit with much reduced efficiency. In fact, binding of PCB to the C494A mutant generates a biliprotein with absorption and RR spectra nearly identical to more typical Phys such as *Syn*-Cph1 and *SyB*-Cph1, which bind PCB via a single thioether linkage involving the C3^1 carbon (9, 31). The assembly of the C494A mutant is more robust than the C522A mutant, suggesting that binding of PCB to Cys-522 via the A-ring ethylidene side chain is thermodynamically favored as compared with PCB binding to Cys-494 at the C4/5 site. In denaturation experiments, we detected a PCB-like adduct associated with the C522A apoprotein but released upon denaturation, which could reflect either photoisomerized and released PVB or PCB non-covalently bound to the apoprotein in the absence of the Cys-522 ligation site.

By a number of criteria, *Te*-PixJ and probably other cyanochromes appear to be photochemically similar to canonical Phys despite differences in their bilins, in their binding architectures, and in their GAF domain sequences. In fact, we found that a number of residues demonstrated to be critical for the photochemistry of canonical Phys (8, 42, 43) may play similar roles in cyanochromes. These include Asp-492, Tyr-493, His-523, His-553, and Arg-507 (Fig. 3). According to our alignments and the predicted three-dimensional model of *Te*-PixJ(Cyc-GAF), Asp-492 appears to be in a similar position to the aspartic acid in the conserved DIP motif in canonical red-absorbing Phys. The DIP aspartate is central to the extensive hydrogen-bond lattice involving the pyrrole nitrogens, the central pyrrole water, and His-523 and appears to be critical for the deprotonation/reprotonation cycle of the chromophore during Pr → Pfr photoconversion (42, 43). Similar to canonical Phys, substitutions of Asp-492 block Pb → Pg photoconversion and generate highly fluorescent variants.

Also paralleling canonical Phys, substitution of Tyr-463 for histidine does not affect bilin incorporation or formation of the ground state (Pb) but does impair photoconversion to the activated form (Pg). Although replacements of the equivalent tyrosine in *Syn*-Cph1 and PhyA and PhyB from the higher plant *Arabidopsis thaliana* generate intensely fluorescent biliproteins (52, 53, 56), similar replacements in the *Te*-PixJ and the PAS-less Phy *SyB*-Cph1 are poorly fluorescent (this report and Ref. 31). This disparity further supports the hypothesis that this tyrosine has different roles among the various Phy clades (57). Arg-507 in *Te*-PixJ was modeled in a similar position as Arg-101 of *SyB*-Cph1. In *SyB*-Cph1, Arg-101 has little impact on the absorption spectrum of Pr and Pfr or photointerconversion but substantially stabilizes the Pfr form against thermal reversion (8). In *Te*-PixJ(Cyc-GAF), replacement of Arg-507 with an alanine dramatically altered the absorption spectrum of the chromoprotein in the dark-adapted state and blocked its photoconversion, indicating that this residue has a much more pronounced effect in cyanochromes. Finally, our model identified two histidines (His-523 and His-553) near the chromophore of *Te*-PixJ. In canonical Phys, comparable histidines are essential for proper photochemistry, presumably by participating in the hydrogen-bond lattice involving the pyrrole nitrogens and interacting with the D ring, respectively (4, 5, 42, 43). Although not analyzed here, we expect that these residues play similar roles in *Te*-PixJ.

As is the presumed case for canonical Phys (1, 4, 5, 7), the experimental RR spectra of *Te*-PixJ are consistent with a *ZZZssa* to *ZZEssa* isomerization at the C15=C16 methine bridge of PVB during photoconversion. Concomitant changes in the environment of the D ring are supported by NMR spectra for *Te*-PixJ(Cyc-GAF) labeled at the C19 carbon with ^{13}C or at the pyrrole nitrogens with ^{15}N. The ^{13}C spectra clearly show that the carbonyl of this pyrrole ring undergoes a chemical shift change upon photoconversion, whereas the ^{15}N spectra identify a single pyrrole as changing its environment, which by default we assign to the D ring based on the ^{13}C data. The large ^{1}H-^{15}N chemical shift change assigned to the D-ring amide could be due to either a hydrogen bond breaking in Pb and re-forming in Pg or possibly a substantial geometric strain of a hydrogen bond that results in simultaneous ^{15}N shielding and ^{1}H deshielding. Both scenarios are compatible with the predicted *Z* to *E* rotation of the C15=C16 methine bridge for Phys, but this rotation remains to be experimentally confirmed.

Two-dimensional NMR with the *Te*-PixJ(Cyc-GAF) domain labeled with ^{15}N revealed numerous rearrangements of the polypeptide during Pb → Pg photoconversion similar to that

seen for the GAF domain from the PAS-less Phy *SyB*-Cph1 during Pr → Pfr photoconversion (31). Although these rearrangements could reflect conformational changes in its backbone and secondary structure upon photoconversion, IR data imply that changes in amino acid side chain conformations predominate.

The distinct absorption spectra of Pb and Pg suggested that Pb → Pg photoconversion of *Te*-PixJ is nearly complete with little residual Pb present after saturating irradiation with blue light. This was confirmed by comparison of the ^{1}H-^{15}N HSQC NMR spectra for dark adapted and blue light-irradiated samples. Many of the chemical shifts seen in the Pb samples were absent in the Pg samples, indicating that little or no Pb remained. Thus, cyanochromes offer the unique opportunity to examine the two photochromic states of a Phy in isolation without substantial contributions from the other spectral form. An exciting possibility is that cyanochromes could be used to generate crystallographic, NMR, or single particle electron microscopic structures of the photoactivated wild-type form of a Phy, which has been hampered in canonical Phys by the residual dark-adapted Pr form substantially contaminating the preparations.

Like canonical Phys, we and Rockwell *et al.* (24) found that cyanochromes become highly fluorescent when photochemically impaired by various mutations affecting the bilin-binding pocket. Here, we found that several Asp-492 variants are intensely green/yellow fluorescent with peak emissions around 578 nm, whereas the Cys-494 substitutions are intensely orange/red fluorescent with peak emissions around 650 nm. In addition to being potentially useful fluorophores by themselves, this overlap in excitation and emission spectra offers the attractive scenario where these fluorophores could be combined for fluorescence resonance energy transfer approaches. For example, the emission spectra of the D494H and C522A mutations of *Te*-PixJ overlap well with the excitation spectra of the various Cys-494 mutations or with the D86H mutation of *SyB*-Cph1, which have excitation and emission spectra at 620 and 650 nm, respectively (31) (Fig. 8*C*), suggesting that efficient energy transfer from one to the other is possible. The attractiveness of the *Te*-PixJ-type fluorophores is also enhanced by their presumed heat stability and their small size, which for *Te*-PixJ requires just the 177-amino acid GAF domain by itself for efficient bilin assembly and fluorescence. Cyanochromes in combination with the recently discovered IR-emitting Phys should enhance the repertoire of research tools in the growing field of bilin-based fluorescence reporters (31, 58, 59).

Exhaustive searches of the various microbial genome data bases with the Cyc-GAF sequence of *Syn*-PixJ and *Te*-PixJ found a number of cyanochrome representatives in cyanobacteria but none outside of this phylum. In evolutionary context, this restriction suggests that cyanochromes evolved from Cphs after the divergence of cyanobacteria from other bacterial phyla, likely to meet the special photobiological needs of these organisms. Their closest relatives are the PAS-less Phys that includes *SyB*-Cph1, a clade that also appears to be restricted to cyanobacteria (supplemental Fig. 1) (31). Although the PAS-less Phys are *a priori* absent an N-terminal PAS domain, only a portion of the cyanochromes appears to be without this domain. One consistent difference between canonical/PAS-less Phys and cyanochromes is the absence in cyanochromes of the insertion between the β3 strand and α3. In canonical Phys, this sequence forms the lasso portion of the knot that connects the PAS and GAF domains (4–7, 9). Without the PAS domain, this region forms a solvent-exposed flexible domain in PAS-less Phys (8).

Another main difference is the apparent absence of a PHY domain downstream of the GAF domain in cyanochromes. The PHY domain is essential for full Pr to Pfr photoconversion and the thermal stability of Pfr in canonical Phys (1, 3). Intriguingly, the two PAS-less Phys studied thus far, *SyA*-Cph1 and *SyB*-Cph1, are less reliant on the PHY domain for Pr → Pfr photoconversion as compared with canonical Phys (31), suggesting that PAS-less Phys deemphasized the need for the PHY domain that proceeded further in cyanochromes, culminating with the complete loss of this domain. Taken together, some cyanochromes can bind bilins and generate their photochromic behavior with only the GAF domain, making their photosensory module the smallest known in the Phy superfamily.

Two well studied Phy-like proteins cluster phylogenetically in the cyanochrome clade: *Syn*-PixJ (TaxD1) that regulates phototaxis toward blue light (26, 27) and *S. elongatus* CikA that is involved in blue light entrainment of the circadian rhythm (47). At least for RcaE, its blue-shifted absorption better overlaps with the absorption of the photosynthetic pigments phycocyanin and phycoerythrin and thus better adjust the abundances of these two photosynthetic accessory complexes to the ambient light environment. Like *Te*-PixJ, both the RcaE and the CikA apoproteins display a strong preference of PCB over BV (60, 61). Similarly, they also assemble poorly with purified PCB *in vitro*, suggesting that *in vivo* assembly systems should be used when attempting to generate large quantities of fully assembled cyanochromes.

Also in the cyanochrome clade is *Syn*-Etr1, previously shown to bind ethylene via a binding pocket sandwiched between two predicted transmembrane domains (40). Using our recombinant assembly system, we found that *Syn*-Etr1 readily bound PCB to generate a blue/green light photochromic biliprotein. Based on the structural organization of this receptor, it is plausible that its histidine kinase output domain is controlled by both ethylene and light as a way to integrate chemical and light signals. Interestingly, it has been reported that ethylene is produced naturally in seawater by photooxidation of dissolved organic carbons (62). Thus, it is possible that abiotically derived ethylene provides a second indirect sensory input for cyanobacteria seeking to optimize light capture.

Acknowledgments—We thank Dr. Sarah Paterson for the Syn-Etr1-containing plasmid and Dr. Katrina Forest for helpful discussions. This study made use of the NMRFAM, which is supported by National Institutes of Health Grants P41RR02301 (Biomedical Research Technology Program/National Center for Research Resources (BRTP/NCRR)) and P41GM66326 (NIGMS). Additional equipment was purchased with funds from the University of Wisconsin-Madison, the National Institutes of Health (Grants RR02781 and RR08438), the National Science Foundation (Grants DMB-8415048, OIA-9977486, and BIR-9214394), and the United States Department of Agriculture.

REFERENCES

1. Rockwell, N. C., Su, Y. S., and Lagarias, J. C. (2006) *Annu. Rev. Plant Biol.* **57,** 837–858
2. Vierstra, R. D., and Karniol, B. (2005) in *Handbook of Photosensory Receptors* (Briggs, W. R., and Spudich, J. L., eds) pp. 171–196, Wiley-VCH Press, Weinheim, Germany
3. Karniol, B., Wagner, J. R., Walker, J. M., and Vierstra, R. D. (2005) *Biochem. J.* **392,** 103–116
4. Wagner, J. R., Brunzelle, J. S., Forest, K. T., and Vierstra, R. D. (2005) *Nature* **438,** 325–331
5. Wagner, J. R., Zhang, J., Brunzelle, J. S., Vierstra, R. D., and Forest, K. T. (2007) *J. Biol. Chem.* **282,** 12298–12309
6. Yang, X., Stojkovic, E. A., Kuk, J., and Moffat, K. (2007) *Proc. Natl. Acad. Sci. U.S.A.* **104,** 12571–12576
7. Yang, X., Kuk, J., and Moffat, K. (2008) *Proc. Natl. Acad. Sci. U.S.A.* **105,** 14715–14720
8. Cornilescu, G., Ulijasz, A. T., Cornilescu, C. C., Markley, J. L., and Vierstra, R. D. (2008) *J. Mol. Biol.* **383,** 403–413
9. Essen, L. O., Mailliet, J., and Hughes, J. (2008) *Proc. Natl. Acad. Sci. U.S.A.* **105,** 14709–14714
10. Mizutani, Y., Tokutomi, S., and Kitagawa, T. (1994) *Biochemistry* **33,** 153–158
11. Andel, F., 3rd, Lagarias, J. C., and Mathies, R. A. (1996) *Biochemistry* **35,** 15997–16008
12. Rüdiger, W., Thümmler, F., Cmiel, E., and Schneider, S. (1983) *Proc. Natl. Acad. Sci. U.S.A.* **80,** 6244–6248
13. Mroginski, M. A., Murgida, D. H., von Stetten, D., Kneip, C., Mark, F., and Hildebrandt, P. (2004) *J. Am. Chem. Soc.* **126,** 16734–16735
14. van Thor, J. J., Mackeen, M., Kuprov, I., Dwek, R. A., and Wormald, M. R. (2006) *Biophys. J.* **91,** 1811–1822
15. Yeh, K. C., Wu, S. H., Murphy, J. T., and Lagarias, J. C. (1997) *Science* **277,** 1505–1508
16. Bhoo, S. H., Davis, S. J., Walker, J., Karniol, B., and Vierstra, R. D. (2001) *Nature* **414,** 776–779
17. Yeh, K. C., and Lagarias, J. C. (1998) *Proc. Natl. Acad. Sci. U.S.A.* **95,** 13976–13981
18. Wu, S. H., and Lagarias, J. C. (2000) *Biochemistry* **39,** 13487–13495
19. Karniol, B., and Vierstra, R. D. (2003) *Proc. Natl. Acad. Sci. U.S.A.* **100,** 2807–2812
20. Giraud, E., Fardoux, J., Fourrier, N., Hannibal, L., Genty, B., Bouyer, P., Dreyfus, B., and Verméglio, A. (2002) *Nature* **417,** 202–205
21. Giraud, E., Zappa, S., Vuillet, L., Adriano, J. M., Hannibal, L., Fardoux, J., Berthomieu, C., Bouyer, P., Pignol, D., and Verméglio, A. (2005) *J. Biol. Chem.* **280,** 32389–32397
22. Yoshihara, S., Katayama, M., Geng, X., and Ikeuchi, M. (2004) *Plant Cell Physiol.* **45,** 1729–1737
23. Hirose, Y., Shimada, T., Narikawa, R., Katayama, M., and Ikeuchi, M. (2008) *Proc. Natl. Acad. Sci. U.S.A.* **105,** 9528–9533
24. Rockwell, N. C., Njuguna, S. L., Roberts, L., Castillo, E., Parson, V. L., Dwojak, S., Lagarias, J. C., and Spiller, S. C. (2008) *Biochemistry* **47,** 7304–7316
25. Narikawa, R., Fukushima, Y., Ishizuka, T., Itoh, S., and Ikeuchi, M. (2008) *J. Mol. Biol.* **380,** 844–855
26. Bhaya, D., Takahashi, A., and Grossman, A. R. (2001) *Proc. Natl. Acad. Sci. U.S.A.* **98,** 7540–7545
27. Yoshihara, S., Suzuki, F., Fujita, H., Geng, X. X., and Ikeuchi, M. (2000) *Plant Cell Physiol.* **41,** 1299–1304
28. Ishizuka, T., Shimada, T., Okajima, K., Yoshihara, S., Ochiai, Y., Katayama, M., and Ikeuchi, M. (2006) *Plant Cell Physiol.* **47,** 1251–1261
29. Ikeuchi, M., and Ishizuka, T. (2008) *Photochem. Photobiol. Sci.* **7,** 1159–1167
30. Ishizuka, T., Narikawa, R., Kohchi, T., Katayama, M., and Ikeuchi, M. (2007) *Plant Cell Physiol.* **48,** 1385–1390
31. Ulijasz, A. T., Cornilescu, G., von Stetten, D., Kaminski, S., Mroginski, M. A., Zhang, J., Bhaya, D., Hildebrandt, P., and Vierstra, R. D. (2008) *J. Biol. Chem.* **283,** 21251–21266
32. Thompson, J. D., Higgins, D. G., and Gibson, T. J. (1994) *Nucleic Acids Res.* **22,** 4673–4680
33. Pollastri, G., Przybylski, D., Rost, B., and Baldi, P. (2002) *Proteins* **47,** 228–235
34. Cheng, J., Randall, A. Z., Sweredoski, M. J., and Baldi, P. (2005) *Nucleic Acids Res.* **33,** W72–76
35. Schwede, T., Kopp, J., Guex, N., and Peitsch, M. C. (2003) *Nucleic Acids Res.* **31,** 3381–3385
36. Chenna, R., Sugawara, H., Koike, T., Lopez, R., Gibson, T. J., Higgins, D. G., and Thompson, J. D. (2003) *Nucleic Acids Res.* **31,** 3497–3500
37. Ronquist, F., and Huelsenbeck, J. P. (2003) *Bioinformatics* **19,** 1572–1574
38. Page, R. D. (1996) *Comput. Appl. Biosci.* **12,** 357–358
39. Felsenstein, J. (1989) *Cladistics* **5,** 164–166
40. Rodríguez, F. I., Esch, J. J., Hall, A. E., Binder, B. M., Schaller, G. E., and Bleecker, A. B. (1999) *Science* **283,** 996–998
41. Gambetta, G. A., and Lagarias, J. C. (2001) *Proc. Natl. Acad. Sci. U.S.A.* **98,** 10566–10571
42. Wagner, J. R., Zhang, J., von Stetten, D., Günther, M., Murgida, D. H., Mroginski, M. A., Walker, J. M., Forest, K. T., Hildebrandt, P., and Vierstra, R. D. (2008) *J. Biol. Chem.* **283,** 12212–12226
43. von Stetten, D., Seibeck, S., Michael, N., Scheerer, P., Mroginski, M. A., Murgida, D. H., Krauss, N., Heyn, M. P., Hildebrandt, P., Borucki, B., and Lamparter, T. (2007) *J. Biol. Chem.* **282,** 2116–2123
44. Kneip, C., Hildebrandt, P., Schlamann, W., Braslavsky, S. E., Mark, F., and Schaffner, K. (1999) *Biochemistry* **38,** 15185–15192
45. Magdo, I., Nemeth, K., Mark, F., Hildebrandt, P., and Schaffner, K. (1999) *J. Phys. Chem. A* **103,** 289–303
46. Delaglio, F., Grzesiek, S., Vuister, G. W., Zhu, G., Pfeifer, J., and Bax, A. (1995) *J. Biomol. NMR* **6,** 277–293
47. Schmitz, O., Katayama, M., Williams, S. B., Kondo, T., and Golden, S. S. (2000) *Science* **289,** 765–768
48. Karniol, B., and Vierstra, R. D. (2006) in *Photomorphogenesis in Plant and Bacteria: Function and Signal Transduction Mechanisms* (Schafer, E., and Nagy, F., eds) pp. 65–98, Springer, Dordrecht, The Netherlands
49. Vierstra, R. D., and Quail, P. H. (1983) *Plant Physiol.* **72,** 264–267
50. Mroginski, M. A., Murgida, D. H., and Hildebrandt, P. (2006) *J. Phys. Chem. A* **110,** 10564–10574
51. Zhao, K. H., and Scheer, H. (1995) *Biochim. Biophys. Acta* **1228,** 244–253
52. Fischer, A. J., and Lagarias, J. C. (2004) *Proc. Natl. Acad. Sci. U.S.A.* **101,** 17334–17339
53. Fischer, A. J., Rockwell, N. C., Jang, A. Y., Ernst, L. A., Waggoner, A. S., Duan, Y., Lei, H., and Lagarias, J. C. (2005) *Biochemistry* **44,** 15203–15215
54. Strauss, H. M., Hughes, J., and Schmieder, P. (2005) *Biochemistry* **44,** 8244–8250
55. Kehoe, D. M., and Grossman, A. R. (1996) *Science* **273,** 1409–1412
56. Su, Y. S., and Lagarias, J. C. (2007) *Plant Cell* **19,** 2124–2139
57. Rockwell, N. C., Shang, L., Martin, S. S., and Lagarias, J. C. (2009) *Proc. Natl. Acad. Sci. U.S.A.* **106,** 6123–6127
58. Shu, X., Royant, A., Lin, M. Z., Aguilera, T. A., Lev-Ram, V., Steinbach, P. A., and Tsien, R. Y. (2009) *Science* **324,** 804–807
59. Miller, A. E., Fischer, A. J., Laurence, T., Hollars, C. W., Saykally, R. J., Lagarias, J. C., and Huser, T. (2006) *Proc. Natl. Acad. Sci. U.S.A.* **103,** 11136–11141
60. Mutsuda, M., Michel, K. P., Zhang, X., Montgomery, B. L., and Golden, S. S. (2003) *J. Biol. Chem.* **278,** 19102–19110
61. Terauchi, K., Montgomery, B. L., Grossman, A. R., Lagarias, J. C., and Kehoe, D. M. (2004) *Mol. Microbiol.* **51,** 567–577
62. Wilson, D. F., Swinnerton, J. W., and Lamontagne, R. A. (1970) *Science* **168,** 1577–1579